ANALYSIS OF THE INTERACTION OF A WEAK NORMAL SHOCK WAVE WITH A TURBULENT BOUNDARY LAYER

R. E. Melnik, et al

Grumman Aerospace Corporation

Prepared for:

Office of Naval Research
National Aeronautics and Space Administration

June 1974

DISCLAIMER NOTICE

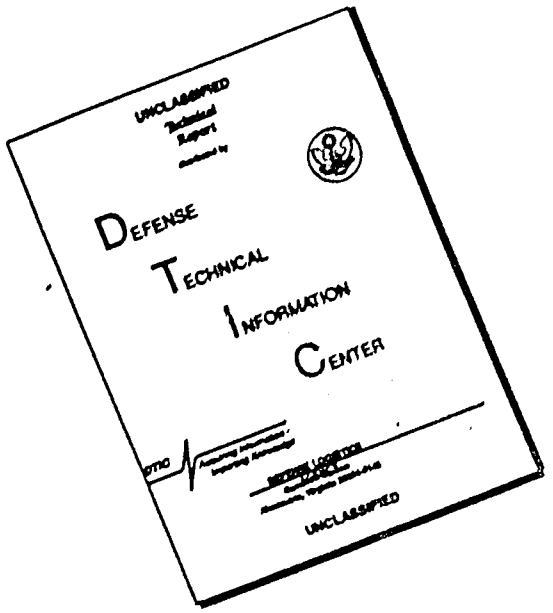

THIS DOCUMENT IS BEST QUALITY AVAILABLE. THE COPY FURNISHED TO DTIC CONTAINED A SIGNIFICANT NUMBER OF PAGES WHICH DO NOT REPRODUCE LEGIBLY.

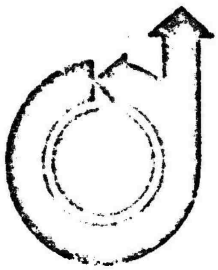

AIAA Paper
No. 74-598

ANALYSIS OF THE INTERACTION OF A WEAK NORMAL SHOCK WAVE WITH A TURBULENT BOUNDARY LAYER

by
R. E. MELNIK and B. GROSSMAN
Grumman Aerospace Corporation
Bethpage, New York

Approved for public release; distribution unlimited.

Grumman Contract Report

AIAA 7th Fluid and Plasma Dynamics Conference
PALO ALTO, CALIFORNIA / JUNE 17-19, 1974

061-191

ANALYSIS OF THE INTERACTION OF A WEAK NORMAL SHOCK WAVE WITH A TURBULENT BOUNDARY LAYER†

R. E. Melnik* and B. Grossman**
Grumman Aerospace Corporation, Bethpage, N. Y.

Abstract

The method of matched asymptotic expansions is used to analyze the interaction of a normal shock wave with an unseparated turbulent boundary layer on a flat surface at transonic speeds. The theory leads to a three-layer description of the interaction in the double limit of Reynolds number approaching infinity and Mach number approaching unity. The interaction involves an outer, inviscid rotational layer, a constant shear-stress wall layer, and a blending region between them. The pressure distribution is obtained from a numerical solution of the outer-layer equations by a mixed-flow relaxation procedure. An analytic solution for the skin friction is determined from the inner-layer equations. The significance of the mathematical model is discussed with reference to existing experimental data.

Nomenclature

a	$=\sqrt{m_e/1+m_e}$
a_1	constant in Bradshaw's model, usually 0.15
B	Law of the wall profile parameter
C_f	skin friction coefficient, $=\tau_w^*/\frac{1}{2}\rho_\infty^* u_\infty^{*2}$
C_2	function determined from blending-layer solution, eq. (5.28)
D	damping factor, eq. (6.1)
e	turbulent kinetic energy
E	perturbation turbulent kinetic energy in blending layer
F	wall layer Reynolds stress function, eq. (6.13)
g_1	defined by eq. (A.7)
H	defined by eq. (5.14)
K	viscosity function, eq. (6.9)
K_t	$=\dfrac{M_\infty^2-1}{\epsilon M_\infty^4}$, transformed interaction parameter
$\bar{K}_t$	$=K_t/\gamma+1$, interaction similarity parameter
L	reference length
L_d	dissipation length
M	Mach number
m_e	$=\dfrac{\gamma-1}{2}M_e^2$
p	pressure
$\bar{p}$	$=\dfrac{\gamma+1}{\chi_t}p_1$, transformed perturbation pressure in outer region
P	perturbation pressure in blending layer
q	$=\sqrt{\dfrac{1-a^2}{a^2}}\sin^{-1}a$
R	wall layer density function, eq. (6.14)
Re_L	$=\rho_\infty^* u_\infty^* L^*/\mu_\infty^*$, Reynolds number
Re_{δ_e}	$=\rho_\infty^{*2}u_\infty^{*2}\delta_1^*/\mu_\infty^*$, Reynolds number based on boundary-layer thickness upstream of the interaction
T	temperature
u	velocity in the $\bar{x}$ direction
u^+	wall layer velocity function, eq. (6.4)
u_1	defect velocity in the outer region upstream of the interaction
u_1^+	u^+ evaluated upstream of the interaction
$\tilde{u}$	Van Driest generalized velocity, eq. (3.1),
$\tilde{u}_e$	$\dfrac{1}{a}\sin^{-1}a$
U	perturbation velocity in x direction in the blending layer
u_τ	$=\sqrt{\tau_w/\rho_w}$, friction velocity
v	velocity in the $\bar{y}$ direction
V	perturbation velocity in y direction in the blending layer
x^*	coordinate parallel to the plate
$\bar{x}$	$=x^*/L^*$
x	stretch $\bar{x}$ coordinate defined in eq. (4.1)
$\tilde{x}$	$x/\sqrt{\chi_t}$
y^*	coordinate normal to the plate
$\bar{y}$	$=y^*/L^*$
y	stretch $\bar{y}$ coordinate in outer region, eq. (4.2)
Y	stretched $\bar{y}$ coordinate in blending layer, eq. (5.6)
y^+	stretched $\bar{y}$ coordinate in the inner layer, eq. (3.9)
α	Bradshaw's mean dilatation parameter
γ	ratio of specific heats, $=1.4$

†The latter phase of this research was partially supported by the Office of Naval Research under Contract N00014-71-C0336. Some of the ideas regarding the turbulence structure were developed in conjunction with NASA Contract NAS 1-12426.

*Director of Aerophysics, Research Department
**Research Scientist

Γ	perturbation Reynolds stress in blending layer
δ	boundary layer thickness
Δ_e	$= M_\infty^2 - 1$, shock strength parameter
Δ_x	x length scale
Δ_y	y length scale
ϵ	$= \sqrt{C_{f_0}/2}$, nondimensional friction velocity upstream of the interaction
ξ	$= 1/\epsilon^2 Re_L$
ϵ_d	turbulent dissipation function
η	y coordinate in the computational plane, eq. (7.16)
κ	Von Karman constant, $= 0.41$
λ	$= -(\chi_t + 2u_{t_1} + \rho_{t_1})/\gamma + 1$
$\bar{\lambda}$	$= \lambda/\chi_t$
μ	coefficient of viscosity
ξ	x coordinate in the computational plane, eq. (7.15)
$\bar{\pi}$	Law of the wake profile parameter
ρ	density
ρ_{t_1}	$= 2m_e u_{t_1}$, defect density in outer layer upstream of the interaction
σ	defined in eq. (5.23)
τ	Reynolds stress
ϕ	velocity potential for first-order outer solution, eqs. (4.12), (4.13)
$\phi_{1,2}$	split velocity potential, eqs. (7.11), (7.12)
$\bar{\phi}$	$= (\gamma+1)\phi/\chi_t^{3/2}$
χ_t	$= M_\infty^2 - 1/\epsilon$ interaction parameter
ω	relaxation parameter
Ω	generalized potential function in the blending layer, eq. (5.29), eq. (5.30)

Subscripts

∞	free stream conditions
0	conditions upstream of the interaction
w	wall condition
1, 2	perturbation indices

Superscripts

*	dimensional quantity
'	turbulent fluctuation

I. Introduction

Interactions between shock waves and turbulent boundary layers occur in a number of practical aerodynamic situations. Examples include supercritical flows over airfoils, exhaust nozzles, and inlets. These interactions often lead to premature separation that can cause severe flow problems such as buffeting, inlet flow-field distortion, and excessive boattail drag. Shock wave-boundary layer interactions are also known to be a major source of significant scale (Reynolds number) effects observed in transonic wind-tunnel tests.

In the present investigation, we apply asymptotic and numerical methods to the solution of the interaction of a normal shock wave with a turbulent boundary layer. We restrict our analysis to the simplest case of a weak shock wave impinging upon a smooth flat plate. The shock strength is assumed to be sufficiently small as to preclude boundary-layer separation, and for standard transonic approximations to apply in the inviscid part of the flow field. We also assume that the Reynolds number is large and that the profile of the approaching turbulent boundary layer is fully developed. Because of these assumptions, the present study should be viewed as a first step towards the solution of more important problems involving separation, stronger shock waves, and flows over curved surfaces. It is hoped that the present effort will lead to a theoretical framework that can eventually include these effects.

Although numerous experimental and analytical investigations of turbulent interactions have been conducted over the past few decades, our understanding of the general problem area remains incomplete, even for the basic case considered here (see Ref. 1 for a review of the shock wave-turbulent boundary layer interaction literature).

A basis for a rational treatment of turbulent interacting flows was established in a pioneering study by Lighthill[2] in 1953. In that work, a two-layer model of an interacting turbulent boundary layer was developed, which was based on preceding efforts by Howarth,[3] and Tsien and Finston.[4] Lighthill's model assumed that the streamwise length scale is small at high Reynolds numbers, so that molecular and turbulent stresses could be neglected over most of the boundary layer. This leads to a two-layer description of an interacting turbulent boundary layer: an outer inviscid, rotational layer where normal pressure gradients are important, and an inner viscous layer required to satisfy the no-slip condition at the surface. Although the model was proposed by Lighthill over 20 years ago, the structure of the inner layer and details of the matching of the inner and outer solutions have not been clarified. It is interesting to note that the general ideas of the Lighthill model served as a basis for the development of rational, asymptotic methods for laminar flows (e.g., Refs. 5–10).

Recently, the two-layer model was employed by Roshko and Thomke,[11] and Elfstrom[12] to treat the supersonic turbulent interaction in a wedge compression corner. About the same time, Watson, Murphy, and Rose,[13] and Rose[14] applied the model to interaction with oblique shock waves.

In Ref. 11 and 13 calculations, the inner layer was ignored and the solution of the outer, rotational inviscid layer was solved by the method of characteristics. (Reference 12 used a semi-analytic method to solve the supersonic region.) In all these calculations, the initial profile had to be cut off arbitrarily to ensure that the flow remained supersonic in the outer region. Experimental data presented in these studies clearly indicate that the rise in surface pressure occurs in two stages. First, the pressure rises nearly discontinuously to a clearly defined level over a streamwise distance of a boundary-layer thickness or less. This is followed by a gradual increase in pressure to an asymptotic value far downstream of the interaction. In some cases overshoots were observed. The computations treated the initial pressure rise as a discontinuity. Comparisons with the experiments indicated that good agreement for the surface-pressure distribution could be obtained if the cutoff was chosen to match the pressure at the downstream end of the initial pressure rise. These results give support to the main features of the two-layer model and demonstrates the usefulness of representing the outer part of the boundary layer by a rotational inviscid flow. However, the two-layer model in its present form is incomplete. It does not treat the flow in the initial pressure rise, nor consider the structure of the flow in the inner layer and its effect on the outer solution. As a result there is little indication of how the slip velocity should, even in principle, be determined.

For the transonic interactions being considered in the present study, the overall pressure rise is more gradual with the result that it can be described using a single streamwise length scale. This is, essentially, because the sonic line occurs in the main part of the boundary layer, well away from the wall, when the free stream Mach number is close to one. We will be able to obtain a complete solution for the surface pressure distribution without an empirical velocity cutoff.

The present analysis is based on the application of the method of matched asymptotic expansions to the full Navier-Stokes equations in the limit of large Reynolds number and Mach number approaching one (weak, normal shock waves). We show that these limits lead to a three-layer description of the boundary layer including an inviscid outer region, a dissipative inner region, and a blending region between them. The analysis can be viewed as a natural extension of the asymptotic theories of Mellor,[15] Yajnik,[16] Bush and Fendell[17,18] for incompressible, and Afzal[19] for compressible non-interacting turbulent boundary layers. These authors show that the conventional defect and law of the wall description of a turbulent profile are related to asymptotic solutions of the Navier-Stokes equations.

Our theoretical model differs from Lighthill's in the defect (outer) region mainly due to appearance of an additional non-linear term in the equation of motion due to transonic considerations. In addition, we note that the initial profile can be expanded in small defect form for large Reynolds numbers. This significantly simplifies the problem, since it allows us to represent the solution in the defect region as a small perturbation to a weakly sheared oncoming stream. A velocity potential can be introduced and the governing equation can be written in a form suitable for numerical solution by mixed flow relaxation procedures, first developed by Murman and Cole.[20]

A similar approach to turbulent interaction problems based on the method of matched asymptotic expansions has been carried out by Adamson and Feo.[21] Their results apply to much weaker shock waves than those considered in the present study. They applied the theory to interactions of very weak oblique shock waves and showed that normal pressure gradients could be ignored in the defect layer. (This is not true for the stronger shocks considered here.) They also derived an analytic expression for the solution to a turbulent free interaction. In our presentation, we show that our outer-layer equations reduce to those of Ref. 21 in the limit as a normalized shock strength parameter approaches zero. The description of the inner layer differs only in that Adamson and Feo employ an eddy viscosity model of the Reynolds stress, whereas the present work uses a turbulent kinetic energy approach. The results of our analysis agree with their estimate of the pressure rise for incipient separation and that this pressure rise should be independent of Reynolds number (for the large Reynolds numbers considered).

We note that Inger and Mason[22] have recently considered the extension of Lighthill's model to transonic flows and have called attention to the importance of including the non-linear transonic term in the equation of motion.

In the following section, we set out the governing equations and discuss the considerations used to establish the order of magnitude of the mean flow variables and turbulent correlations. The structure of the solution in the double limit of Mach number going to one and Reynolds number approaching infinity, along with the length scales

appropriate to the various regions will be established. Section III considers the solution in the non-interacting part of the boundary layer upstream of the shock wave. Here we will show that the results obtained from the method of matched asymptotic expansions for incompressible flow must be considerably modified to account for compressibility. Section IV considers the outer or defect layer. It will be shown that the flow in this region is governed by a generalization of the usual non-linear transonic potential flow equation and that the solution depends on two similarity parameters. Next, the basic equations governing the blending layer are derived in Section V. We show that history effects are important in this region and suggest specific turbulence models for closing the system of equations. In Section VI, we develop the solution in the wall layer and carry out the matching with the blending layer. A solution for the skin friction is then obtained. The complete boundary value problem for the numerical solution of the outer region is formulated in Section VII. The numerical methods used to solve the problem are discussed in detail. Section VIII contains results of the numerical solution for several normal shock-wave interaction problems along with comparisons and discussions of experimental data. Finally, a summary and a critique of the major findings of this effort, along with a discussion of methods for improving and extending the analysis, are presented in Section IX.

II. Formulation

The flow field under consideration is the interaction of a weak normal shock wave with a turbulent boundary layer on a flat surface as sketched in Fig. 1. For simplicity, the wall is considered to be smooth, adiabatic, and non-porous. We assume the interaction to occur at a distance L^* from the leading edge of the plate and that the flow is uniform upstream of the interaction, outside the boundary layer with velocity u_∞^*, density ρ_∞^*, pressure p_∞^* and viscosity μ_∞^*. (The asterisk denotes dimensional quantities.) These quantities define a Reynolds number

$$Re_L = \frac{\rho_\infty^* u_\infty^* L^*}{\mu_\infty^*} \qquad (2.1)$$

The shock wave is assumed to be normal to the flat plate far above the interaction and can be characterized by the value of a single shock strength parameter, which we take to be

$$\Delta_s = M_\infty^2 - 1 \qquad (2.2)$$

where M_∞ is the uniform Mach number upstream of the shock.

Limit Process

We will consider the solution of this problem in the double limit of

$$Re_L \to \infty \quad \text{and} \quad \Delta_s \to 0 \qquad (2.3)$$

It has been found to be more convenient to arrange the expansion in terms of a parameter ϵ, equal to the non-dimensional friction velocity of the approaching boundary layer, defined as

$$\epsilon = \sqrt{C_{f_0}/2} \qquad (2.4)$$

where C_{f_0} is the skin friction coefficient. Since ϵ may be related to the Reynolds number by the solution of the undisturbed boundary layer, the limit defined in eq. (2.3) may be equivalently written as

$$\epsilon \to 0 \quad \text{and} \quad \Delta_s \to 0 \qquad (2.5)$$

In the limits given in eq. (2.5) (or (2.3)), the boundary-layer thickness vanishes and the shock wave becomes infinitesimally weak. The standard experimental correlations of low-speed turbulent boundary-layer data (e.g., see Ref. 23), and the more recent asymptotic analyses,[15-19] show that the velocity profile has a small defect form at high Reynolds numbers. The velocity differs from free stream by a term of $0(\epsilon)$ over most of the boundary layer. The small defect form of the turbulent profile is an important element in our approach. We will subsequently show that the two limits in eq. (2.5) are not independent in the most general case and that a distinguished limit does exist. This limit can best be defined in terms of a similarity variable, χ_t defined by

$$\chi_t = \frac{M_\infty^2 - 1}{\epsilon} \qquad (2.6)$$

The limit is then assumed to be

$$\left.\begin{matrix}\epsilon \to 0 \\ M_\infty \to 1\end{matrix}\right\} \chi_t \text{ fixed} \qquad (2.7)$$

In this limit, the velocity jump across the shock wave is the same order as the velocity defect in the approaching boundary layer. In the interaction problem of Adamson and Feo,[21] χ_t vanishes and the shock strength is weaker than considered here. At the other extreme the present results, and those in Ref. 21, indicate that the shock strength for incipent separation is $0(1)$, independent of Reynolds number. Thus, it follows that

for separation $\chi_i = O(\epsilon^{-1}) \to \infty$ which is stronger than the shock strength considered here.

Length scales

For the sake of clarity in this section, we will describe the asymptotic structure of the flow field and will give the pertinent length scales in terms of ϵ without mathematical justification. The proof that the suggested length scales are appropriate naturally follows from the substitution of the assumed expansions into the equation of motion and from a careful comparison of the orders of magnitude of the various terms. This part of the analysis is conventional and we will not comment further upon it.

At large Reynolds numbers, the boundary layer spreads the discontinuous pressure rise imposed by the impinging shock wave over a small streamwise distance. There has been some uncertainty in previous studies of turbulent interactions about the magnitude of this interaction length. In the limit situation defined by eq. (2.7), it can be shown that the flow behaves as an inviscid fluid over most of the boundary layer and that the sonic line lies within the main portion of the boundary layer. The vertical extent of the interaction zone is fixed by the upstream flow to be of the order of a boundary layer thickness. For a fully developed turbulent boundary layer, the thickness scales with the friction velocity, and thus

$$\delta_0^*/L^* = O(\epsilon) \tag{2.8}$$

where δ_0^* is the boundary layer thickness upstream of the interaction. With velocity disturbances of $O(\epsilon)$, it follows from conventional transonic considerations that the streamwise length scale is given by

$$\Delta_x = \epsilon^{1/2}\delta_0^* = O(\epsilon^{3/2})L^* \tag{2.9a}$$

As mentioned above, the y ordinate scales as

$$(\Delta_y)_{outer} = \delta_0^* = O(\epsilon)L^* \tag{2.9b}$$

Note that the order of the streamwise length scale is less than a boundary layer thickness. Physically, this follows from the observation that the extent of upstream influence is controlled by the location of the sonic line in the boundary layer. For the present case, consideration of the slope of the characteristics in the upstream flow leads directly to eq. (2.9).

The length scales defined in eq. (2.9) describe the outer or defect region of the interaction, shown schematically in Fig. 2. Under the limit in eq. (2.7) and the above length scales, all turbulent and viscous stresses are negligible. Hence, as in Lighthill's ad hoc model, the flow in this region is governed by rotational inviscid flow equations.

The solution of the inviscid outer-layer equations does not satisfy the no-slip condition at the surface and, hence, at least one additional inner region is required. The present analysis shows that two inner regions are required (as shown in Fig. 2). One is a conventional compressible wall layer. In this region the flow is in local equilibrium, where the solution for the shear stress adjusts instantaneously, in response to changes in velocity at the outer edge. Thus, the impinging shock wave interacts with the main part of the boundary layer and decelerates the flow at the outer edge of the wall layer. This reduction in velocity causes a reduction in shear stress and skin friction in the wall layer. From a consideration of the turbulent kinetic-energy equation, it can be demonstrated that the shear stress in the outer part of the boundary layer is "frozen" at the upstream values (to lowest order in ϵ). Hence, a discontinuity develops between the shear stress in the outer and wall layers. The resolution of this mismatch requires the introduction of a third region called the blending layer. This three-layer structure appears to be characteristic of turbulent boundary layers in a steep pressure gradient.

The length scale for the wall layer is given in terms of the local friction velocity in the usual manner by

$$(\Delta_y)_{wall\ layer} = \mu_w^*(x)/\rho_w^*(x)u_\tau^*(x) = O(\epsilon\hat{\epsilon}) \tag{2.10}$$

where μ_w^* is the local viscosity coefficient, $\rho_w^*(x)$ the local density, and u_τ^* the local friction velocity, all defined with respect to surface values, and $\hat{\epsilon}$ is defined (following Mellor[15]) by

$$\hat{\epsilon} = \frac{1}{\epsilon^2 Re_L} = O[\exp(-1/\epsilon)] \tag{2.11}$$

The length scale in the blending layer is determined by introducing eq. (2.9a) into the streamwise momentum equation together with the requirement that inertia terms and turbulent shear stress terms be of the same order of magnitude near the wall. This leads to the length scale in the blending layer of

$$(\Delta_y)_{blending\ layer} = \epsilon^{3/2}\delta_0^* = O(\epsilon^{5/2})L^* \tag{2.12}$$

Equations (2.8) through (2.12) provide the length scales that are to be used to construct asymptotic expansions of the solution in each of the three regions. It can be noted here that to lowest order in ϵ, normal pressure gradients are negligible in the wall and blending layers. Hence, the pressure distribution through the interaction is obtained from a solution of the outer-layer equations. Also, it will be shown that a solution for the skin friction, to second order, can be obtained from the wall-layer equations with the outer-layer surface pressure imposed. These solutions will be discussed in Sections IV and VI.

Governing Equations

The present formulation is based on the time-averaged Navier-Stokes equations. Since turbulent non-equilibrium or history effects are likely important in steep pressure gradients, we will use Bradshaw's turbulent kinetic-energy formulation[24] in our closure model. However, our analysis will show that the need for a specific closure model first arises in the solution for the second-order problem in the blending layer and affects only the second-order solution for the skin friction.

A large number of turbulent correlations arise in the time-averaged compressible Navier-Stokes equations. We will follow Bradshaw's[24] and Afzal's[19] use of Kistler's[25] data to estimate the order of magnitude of the correlations in terms of the undisturbed friction velocity ϵ and neglect the terms that are of higher order in all three regimes of the present problem. In these papers, it was shown that the fluctuations of velocity, temperature, and density are of $O(\epsilon)$ and the fluctuations in pressure are of $O(\epsilon^2)$. In using these estimates to eliminate certain higher-order correlation terms we must, of course, take note of the small streamwise length scale of the interaction. We also note that the viscous terms are only important in the innermost wall layer where boundary-layer approximations are valid. Hence only the boundary-layer form of the viscous terms in the streamwise momentum equation will be explicitly included. Thus, the governing equations (from Ref. 24) containing only those terms important in any of the three layers are as follows:

$$\text{continuity} \quad \frac{\partial}{\partial \bar{x}}\left(\rho u + \langle \rho' u' \rangle\right) + \frac{\partial}{\partial \bar{y}}\left(\rho \bar{v}\right) = 0 \qquad (2.13)$$

$$\bar{x}\text{-momentum} \quad \left(\rho u + \langle \rho' u' \rangle\right)\frac{\partial u}{\partial \bar{x}} + \rho \bar{v}\frac{\partial u}{\partial \bar{y}} + \frac{\partial p}{\partial \bar{x}} = \frac{1}{Re_\infty}\frac{\partial}{\partial y}\left(\mu \frac{\partial u}{\partial y}\right)$$

$$- \frac{\partial}{\partial \bar{x}}\left(\rho \langle u'u' \rangle + u\langle \rho' u' \rangle\right)$$

$$- \frac{\partial}{\partial \bar{y}}\left(\rho \langle u'v' \rangle + \bar{v}\langle \rho' u' \rangle\right) + O(\epsilon^3) \qquad (2.14)$$

$$\bar{y}\text{-momentum} \quad \left(\rho u + \langle \rho' u' \rangle\right)\frac{\partial \bar{v}}{\partial \bar{x}} + \rho \bar{v}\frac{\partial \bar{v}}{\partial \bar{y}} + \frac{\partial p}{\partial \bar{y}}$$

$$= - \frac{\partial}{\partial \bar{x}}\left(\rho \langle u'v' \rangle\right) -$$

$$\frac{\partial}{\partial \bar{y}}\left(\rho \langle v'v' \rangle\right) + O(\epsilon^3) \qquad (2.15)$$

$$\text{turbulent kinetic energy} \quad \left(\rho u + \langle \rho' u' \rangle\right)\frac{\partial e}{\partial \bar{x}} + \rho \bar{v}\frac{\partial e}{\partial \bar{y}}$$

$$= - \rho \langle u'v' \rangle \frac{\partial u}{\partial \bar{y}}$$

$$- \alpha \rho \langle u'v' \rangle \left(\frac{\partial u}{\partial \bar{x}} + \frac{\partial v}{\partial \bar{y}}\right)$$

$$- \frac{\partial}{\partial \bar{y}}\left(\langle p'v' \rangle + \rho \langle e'v' \rangle + \langle \rho' e'v' \rangle\right) - \rho \epsilon_d + O(\epsilon^3) \qquad (2.16)$$

where the $\langle\ \rangle$ signify mean values. Here $\bar{v}$ is written to include the mass flow correlation and is defined as

$$\rho \bar{v} = \rho v + \langle \rho' v' \rangle \qquad (2.17)$$

(The bar will be omitted from v in all subsequent equations.) The equation of state is written in the form

$$p = \frac{1}{\gamma}\rho T \qquad (2.18)$$

The thermal energy is expressed as a condition of constant total temperature by

$$T + \frac{\gamma - 1}{2}u^2 = \frac{1}{M_\infty^2} + \frac{\gamma - 1}{2} \qquad (2.19)$$

In the above equations u, v, ρ, p, T, μ and γ are respectively, the non-dimensional mean streamwise and normal component of velocity, density, pressure, temperature, viscosity coefficient, and ratio of specific heats. Primes denote non-dimensional fluctuations. The quantity e is the turbulent kinetic energy and ϵ_d is the turbulent dissipation function. Velocities are made non-dimensional with respect to u_∞^*, density with ρ_∞^*, pressure with $\rho_\infty^* U_\infty^{*2}$, temperature with $u_\infty^{*2}/\gamma\mathcal{R}$, ($\mathcal{R}$ being the gas constant), turbulent kinetic energy with u_∞^{*2} and dissipation with u_∞^{*3}/L^*. The coordi-

nates $\bar{x}$ and $\bar{y}$ in the above equations are non-dimensionalized with respect to L^*.

The turbulent kinetic-energy equation explicitly includes certain mean dilatation terms in a form suggested by Bradshaw.[26],[27] The factor a, multiplying these terms in eq. (2.16) is a function of the normal stress correlations $\langle u'u' \rangle$, $\langle v'v' \rangle$ and the density-velocity correlations $\langle \rho'u' \rangle$, $\langle \rho'v' \rangle$. Bradshaw has shown, from a consideration of the magnitude of these terms, that a should be a constant that is approximately $-10/3$. It follows that the above terms will first effect the present solution in the second-order terms of the blending layer. This will have a direct bearing on the second-order skin friction solution. However, as noted in Refs. 26 and 27, the effect of the mean dilatation term in compressible flows with steep pressure gradients can be numerically much larger than their formal order of magnitude would suggest. Bradshaw has also indicated that these effects can be modeled as "extra production terms" through an increase in a. These considerations directly apply to the present problem and suggest that careful consideration of the choice of a will be required to obtain accurate skin-friction solutions.

The form of the thermal energy equation given in eq. (2.19) is a statement that the total temperature is constant. The contribution from the v component of velocity to the total temperature is neglected, as it does not contribute to any order considered in the three regions. This form of the energy equation is a valid approximation for adiabatic walls and for laminar and turbulent Prandtl numbers both equal to one (see Ref. 28*). This approximation is not essential and the present theory can be generalized to include a full treatment of the energy equation.

The above system of equations still includes a rather large number of unknown correlation functions and hence does not form a closed system of equations. However, most of these correlations will drop out of the lower order equations in the three layers in the limit of large Reynolds number (using the fluctuation estimates given previously). The only surviving correlations appear in the second-order equations for the blending layer and these are the ones discussed by Bradshaw.[24],[26] In this region, the pressure diffusion term, as modeled by Bradshaw, is of higher order and can be neglected. Also intermittency corrections need not be considered. These factors significantly simplify the closure problem and make strong interaction problems more tractable than standard boundary-layer problems (from a closure point of view). The specific closure approximation for the few remaining terms will be given in Section V.

In the following sections we will expand the solution in each region in powers of ϵ and $\log\epsilon$. It is important to note that ϵ is related to the Reynolds number through the skin friction solution in the approaching boundary layer. It follows that ϵ is related to Re_L by

$$\epsilon = 0(1/\log Re_L)$$

Thus, the expansions, in terms of Reynolds number, proceed in powers of $(1/\log Re_L)$ and $\log(1/\log Re_L)$. As a result, the approach to a large Reynolds number limit could be very slow. This is undoubtably related to the difficulty in establishing a clear Reynolds number trend in the experimental investigation of strong interaction problems.

To establish a frame of reference, we note that for zero pressure gradient and transonic Mach numbers, ϵ is in the range 0.02–0.04 for $Re_L = 10^6 - 10^7$. Hence ϵ is small enough (though not impressively small) for an asymptotic result to be useful.

III. Initial Profile
(non-interacting boundary layer)

One would expect that the formal asymptotic theories developed for incompressible turbulent flows[15]–[16] could be extended to the compressible boundary layer upstream of the interaction. This solution would then provide initial conditions that are asymptotically consistent with the mathematical description used to solve the interaction problem. Afzal[12] has considered the extension of Yajnik's[16] incompressible solution to compressible turbulent boundary layers. He has shown that the structure of the solution is the same as for incompressible flow. Two layers were required, an outer defect region and an inner wall layer with the same length scales as the incompressible case. Following Yajnik's procedure for incompressible flow, the solution was represented by limit-function expansions for small friction velocity in each region. It was demonstrated that the outer expansion of the inner solution had the same general form as the inner

*Analysis of Rotta's work indicates that the effect of the interaction does not change this conclusion.

expansion of the outer solution. This indicated that there was the possibility of term by term matching of the two expansions. However, Afzal worked with an unclosed system of turbulent equations and did not show that the two expansions did indeed match. In the present study, we were able to show that the expansions employed by Afzal did not match. The difficulty stems from the fact that the density varies by O(1) from wall to free stream values across the wall layer. In the limit-function expansions of Ref. 19, the density is treated as a constant, equal to its wall value, in the lowest-order inner solution. Our results indicate that, although this is a valid asymptotic result, it is not valid in an inner region large enough to overlap the outer region.*

This difficulty can be overcome by using a generalized expansion, which is not a limit-function expansion, to represent the solution in the wall layer. To obtain an overlap, we retain the density terms to all orders. Van Driest[29] has shown how this can be carried out. In his early work, he employed the Prandtl mixing-length theory to model the Reynolds stresses, and computed the density and temperature from a Crocco integral representation. Exact solutions of the resulting equations, valid in the fully turbulent part of the wall layer were obtained for both insulated and non-adiabatic walls.

The Prandtl mixing-length equations can be shown to be an asymptotically consistent result, following from the behavior of the turbulent kinetic-energy equation in the fully turbulent part of the wall layer. Since our assumption of constant total temperature is contained within the Crocco integral representation, Van Driest's solution can be made the basis of a formal asymptotic theory for compressible wall layers. We follow this procedure in developing the wall layer solutions in the interaction region (see Section VI). However, in establishing the initial profile, we found it more convenient to use the Maise-MacDonald[30] (also see Ref. 31) correlations of compressible boundary layer profiles. They employed the Van Driest solution in the form of a transformation from compressible to incompressible profiles. Van Driest's generalized solution for an insulated plate can be written as

$$u = \frac{1}{a}\sin a\bar{u} \qquad (3.1)$$

$$a^2 = \frac{m_e}{1+m_e}, \quad m_e = \frac{\gamma-1}{2}M_e^2 \qquad (3.2)$$

where u is the compressible velocity and $\bar{u}$ is the related incompressible profile. The density and temperature can be obtained from the total temperature (constant in the present analysis) as follows:

$$\frac{\rho_w}{\rho} = \frac{T}{T_w} = 1 - a^2\bar{u}^2 \qquad (3.3)$$

Van Driest's solution for u was valid only in the fully turbulent part of the wall layer. Maise and MacDonald[30] made a significant contribution when they recognized that a large number of compressible profiles can be correlated by identifying u with Coles' law of the wake-law of the wall incompressible correlation.[32] Thus, they assumed that the compressible profile was given by eq. (3.1) with $\bar{u}$ from (using a non-dimensional form of Alber and Coats'[11] notation)

$$\bar{u} = \begin{cases} \bar{u}_e + u_\tau\left[\frac{1}{\kappa}\log y + \frac{\bar{\pi}}{\kappa}(1+\cos\pi y)\right], & y \le 1 \\ \bar{u}_e; & y \ge 1 \end{cases} \qquad (3.4)$$

Equivalently, in inner variables

$$\bar{u} = u_\tau\left[\frac{1}{\kappa}\log y^* + B_0 + \frac{\bar{\pi}}{\kappa}(1-\cos\pi y)\right] \qquad (3.5)$$

where

$$\bar{u}_e = \frac{1}{a}\sin^{-1}a \qquad (3.6)$$

and a is defined by Eq. (3.2) and the Van Karman constant, $\kappa = 0.41$. The quantity u_τ is the non-dimensional friction velocity, based on wall density and is related to our small parameter ϵ by

$$\epsilon = \sqrt{c_{f_{0/2}}} = u_\tau\sqrt{\rho_w} \qquad (3.7)$$

The wall density can be found by evaluating eq. (3.3) in the free stream,

$$\rho_w = 1 - a^2 \qquad (3.8)$$

The inner coordinate y^* is a stretched wall variable defined by

$$y^* = \left(\frac{\rho_w u_\tau \delta_0}{\mu_w}\right)y \qquad (3.9)$$

*This conclusion was also arrived at by Adamson and Feo.[21] A general discussion of this type of matching problem is found in an article by Lagerstrom and Casten.[33]

where δ_0 is the boundary layer thickness. The constants B_0 and $\bar{\pi}$ are the usual ones appearing in Cole's formulation. Thus, $B_0 = 5.0$ and for zero pressure gradients, $\bar{\pi} = 0.5$.

The skin friction law for compressible flow (e.g. Ref. 31) follows from eqs. (3.4) and (3.5) as

$$\frac{\tilde{u}_e}{u_\tau} = \frac{1}{\kappa}\log\left[\frac{\rho_w u_\tau R_{\delta_0}}{\mu_w}\right] + B_0 + \frac{2\bar{\pi}}{\kappa} \qquad (3.10)$$

where R_{δ_0} is the Reynolds number based on boundary-layer thickness and free stream quantities. The Maise-McDonald representation can be viewed as a two-parameter fit of the upstream velocity profile. The two parameters can be our skin friction parameter ϵ and the Cole ' shape parameter $\bar{\pi}$. The skin-friction law then provides an expression for the boundary-layer thickness in terms of ϵ and $\bar{\pi}$. Namely,

$$R_{\delta_0} = \frac{\mu_w}{\epsilon\sqrt{\rho_w}}\exp\left\{\frac{\kappa}{\epsilon}\left[\tilde{u}_e\sqrt{\rho_w} - \left(B_0 + \frac{2\bar{\pi}}{\kappa}\right)\right]\right\}. \qquad (3.11)$$

The Maise-McDonald profile can be written in the form of a limit-function expansion in the defect layer by substituting eq. (3.4) into eq. (3.1) and expanding the result for $\epsilon \to 0$ keeping y fixed. This yields

$$u_{outer} = 1 + \epsilon u_1(y) + \epsilon^2\frac{m_e}{2}u_1^2(y) + \ldots \qquad (3.12)$$

where

$$u_1(y) = \frac{1}{\kappa}\log y - \frac{\bar{\pi}}{\kappa}(1 + \cos\pi y). \qquad (3.13)$$

In Appendix A, we demonstrate that expansion of the Maise-McDonald profile in a limit-function form in the wall layer (i.e. $\epsilon \to 0$, y^+ fixed) results in an inner solution that does not match to the outer solution given in eq. (3.12). We also show that the generalized inner solution for u, formed by the substitution of eq. (3.5) into eq. (3.1), does match to eq. (3.12). Thus, an acceptable (i.e. matchable) two-layer solution for the non-interacting boundary layer is given by the limit function expansion eq. (3.12) for the outer region and by the generalized expansion eqs. (3.11) and (3.5) in the wall layer.

For future reference, we give the outer expansion for the initial density and temperature profiles:

$$\rho = 1 + \epsilon\rho_1(y) + O(\epsilon^2) \quad 1 + \epsilon\, 2m_e u_1(y) + O(\epsilon^2) \qquad (3.14)$$

$$T = \frac{1}{M_e^2}[1 - \epsilon\, 2m_e u_1(y)] + O(\epsilon^2) \qquad (3.15)$$

The density and temperature profiles must be computed in the inner layer from the exact expression given in eq. (3.3), in order that the inner and outer expansions overlap.

We call attention to the fact that the above expansions are not valid in the viscous part of the wall layer. To obtain initial profiles in this region, we would have to extend Van Driest's equations to include viscous terms. Although this appears feasible, it would involve numerical integrations which add considerable complexity to the solution. Fortunately, this part of the initial profile will not be required in the present investigation.

IV. Outer Layer

Details of the flow in the outer or defect region (i.e. see Fig. 2) will now be considered. Stretched variables, x, y are introduced using the length scales defined by eqs. (2.9a,b)

$$x^* = \delta_0^*\epsilon^{1/2}x \qquad (4.1)$$

$$y^* = \delta_0^* y \qquad (4.2)$$

where δ_0^* is the (dimensional) thickness of the approaching boundary layer. It is the only length entering into the problem and can be determined from the velocity profile upstream of the interaction. We introduce these length scales into the governing equations given by eqs. (2.13) through (2.19) and assume the non-dimensional solution in this region can be expanded in the form

$$u = 1 + \epsilon u_1(x, y) + \ldots \qquad (4.3a)$$

$$v = \epsilon^{3/2}v_1(x, y) + \ldots \qquad (4.3b)$$

$$p = p_\infty + \epsilon p_1(x, y) + \ldots \qquad (4.3c)$$

$$\rho = 1 + \epsilon\rho_1(x, y) + \ldots \qquad (4.3d)$$

$$T = T_\infty + \epsilon T_1(x, y) + \ldots \qquad (4.3e)$$

$$\tau = \epsilon^2[\tau_0(y) + O(\epsilon)] \qquad (4.3f)$$

$$e = \epsilon^2[e_0(y) + O(\epsilon)] \qquad (4.3g)$$

where the quantity τ is the non-dimensional Reynolds stress, defined by

$$\tau = -\rho\langle u'v'\rangle \qquad (4.4)$$

The magnitudes of the first-order terms of u, p, ρ and T are determined from the strength of the impinging shockwave; the order of v follows from

mass flow requirements and the transonic length scales given in eqs. (4.1) and (4.2). Effects of turbulent stresses do not enter the expansions for u, v, p, ρ and T until terms of $O(\epsilon^{5/2})$, hence only inviscid equations need be considered to this order. This considerably simplifies the problem, since large numbers of unknown correlations need not be considered in the outer region.

The lowest-order Reynolds stress $\tau_0(y)$ and turbulent kinetic energy $e_0(y)$ are determined, in principle, from the upstream profile. Fortunately these terms are not required to determine the leading terms of the outer solution. Consideration of the advection terms in the turbulent kinetic-energy equation demonstrates that the turbulent stresses are frozen at their upstream values to $O(\epsilon)$ as indicated in eqs. (4.3f) and (4.3g). In the present investigation, only the leading terms in the outer inviscid flow will be considered.

Substitution of eqs. (4.1) through (4.3) into eqs. (2.13) through (2.19) and carrying out the limit $\epsilon \to 0$, χ_t fixed leads to the following set of equations governing the first-order solution:

$$[\chi_t - (\gamma-1)u_1 + \rho_1 + (\gamma+1)u_1]u_{1_x} - v_{1_y} = 0 \qquad (4.5)$$

$$u_{1_y} - v_{1_x} = \frac{du_1}{dy} \qquad (4.6)$$

$$p_1 = u_1(y) - u_1 \qquad (4.7)$$

$$\rho_1 = \rho_1(y) + p_1 \qquad (4.8)$$

$$T_1 = -(\gamma-1)u_1(y) + (\gamma-1)p_1 \qquad (4.9)$$

where the initial density distribution $\rho_1(y)$ is given by eq. (3.14) as

$$\rho_1(y) = (\gamma-1)u_1(y)\,, \qquad (4.10)$$

$u_1(y)$ is the defect part of the initial profile given by eq. (3.13) and χ_t is a transonic turbulent interaction parameter defined in eq. (2.6), repeated below as

$$\chi_t = \frac{M_\infty^2 - 1}{\epsilon} = \frac{M_\infty^2 - 1}{\sqrt{C_{f_0}/2}}\,. \qquad (4.11)$$

Notice that the outer solution exhibits a fundamental similarity in that it only depends upon the two basic parameters ϵ and M_∞ in the combination appearing in the definition of χ_t. This indicates that the solution is similar for fixed values of χ_t.

Equation (4.6) indicates that a potential function can be introduced and the solution for the velocity components expressed the form

$$u_1 = u_1(y) + \phi_x \qquad (4.12)$$

$$v_1 = \phi_y \qquad (4.13)$$

Thus, the solution in the defect region is an irrotational perturbation to a weakly sheared oncoming (rotational) stream. The potential function satisfies the following generalized transonic flow equations:

$$(\gamma+1)[\lambda(y) - \phi_x]\phi_{xx} + \phi_{yy} = 0 \qquad (4.14)$$

where

$$\lambda(y) = -\left[\frac{\chi_t}{\gamma+1} + u_1\right] \qquad (4.15)$$

The boundary conditions for eq. (4.14) can be found by matching to the solution in neighboring regions. For large y, the solution must approach the discontinuous normal shock solution which in the present notation leads to the condition

$$\phi_x = \begin{cases} 0 & x < 0\,, \quad y \to \infty \\ 2\lambda_\infty & x > 0\,, \quad y \to \infty \end{cases} \qquad (4.16)$$

with $\lambda_\infty = -\chi_t/\gamma+1$ and where $x = 0$ is the shock location in the non-interacting inviscid flow. Since the perturbation induced by the interaction must vanish far upstream and downstream of the impingement point, we have

$$\lim_{x \to -\infty} \phi_x(x,y) = 0 \qquad (4.17)$$

$$\lim_{x \to \infty} \phi_x(x,y) = 2\lambda_\infty \qquad (4.18)$$

The formulation of the boundary-value problem is completed by the specification of surface conditions at $y = 0$. This is obtained by matching to the inner-layer solutions in the following two sections. Anticipating the results of these sections, we have

$$\phi_y(x,0) = 0\,. \qquad (4.19)$$

Eq. (4.19) implies that displacement effects induced by the inner layers do not contribute to the v velocity to 0 $(\epsilon^{3/2})$. This will be confirmed in the following sections.

The basic theory, defined by eqs. (4.14) and (4.15) is useful over a limited range of Mach numbers near one (e.g., $M_\infty \leq 1.2$). The accuracy of the theory can be considerably improved by retaining the exact Mach number dependence of

a number of coefficients in the expansion that, formally, should be set equal to these limiting values at $M_\infty = 1$. Specifically, the outer-layer governing equation is generalized to the following:

$$[\chi_t + (\gamma+1)M_\infty^2 u_1 + (\gamma+1)M_\infty^2 \phi_x]\phi_{xx} - \phi_{yy} = 0 \quad . \tag{4.20}$$

The boundary conditions for eq. (4.20) are unchanged except for the far-field normal shock condition given by eq. (4.16). The jump condition associated with eq. (4.20) is

$$\phi_x = \begin{cases} 0 \ , & x<0 \ , \ y-\infty \\ \dfrac{-2\chi_t}{(\gamma+1)M_\infty^2} \ , & x>0 \ , \ y-\infty \end{cases} \tag{4.21}$$

which contains an extra Mach number term. Although the Mach numbers appearing explicitly in eqs. (4.20) and (4.21) could be formally set equal to one, their retention will lead to more accurate solutions. The original equations given in eqs. (4.14) and (4.15) will be referred to as the basic theory while the new equations will be referred to as the extended theory. Improved accuracy arises because the new jump conditions yield the exact value of the static pressure rise behind a normal shock wave. An important feature of the extended theory is that solutions of the new equation can be obtained from a simple transformation of solutions to the basic small-disturbance equation. In Sec. VII, we develop a numerical technique for solving the basic small-disturbance equations given in eqs. (4.14) and (4.15). These can be converted into solutions of the more accurate extended equations through the following transformation. If

$$p_1 = p_1(x, y; K_t) \tag{4.22}$$

is a solution for the pressure obtained from Eqs. (4.14) and (4.15) for a given χ_t equal to K_t, then the solution of the extended equations is given by

$$p_E = p_1(M_\infty x, y; K_t) \tag{4.23}$$

where K_t is related to the Mach number by

$$K_t = \frac{M_\infty^2 - 1}{\epsilon M_\infty^2} \tag{4.24}$$

These transformations provide a simple and direct method for greatly improving the accuracy of the small-disturbance theory. Equation (4.20) also leads to a turbulent similarity theory. For example, it follows from eqs. (4.20) and (4.21) that the pressure coefficient can be written in the form

$$C_p(x^*, y^*; \epsilon, M_\infty, \bar{\kappa}, \gamma) = \epsilon \bar{C}_p(s, y; \bar{K}_t, \bar{\kappa}) \tag{4.25}$$

where s and $\bar{K}_t$ are defined by the relations

$$\frac{x^*}{\delta_\delta^*} = \epsilon^{1/2} x = \epsilon^{1/2} M_\infty (\gamma+1) s \tag{4.26}$$

$$\bar{K}_t = \frac{M_\infty^2 - 1}{\epsilon(\gamma+1)M_\infty^2} \tag{4.27}$$

and where $\bar{C}_p$ is a universal function of s and y for given values of $\bar{K}_t$ and $\bar{\kappa}$. It follows that s and y are the basic non-dimensional coordinates for the problem and $\bar{K}_t$ is a general similarity variable for transonic turbulent interactions. The above similarity applies for the law of the wall-law of the wake form assumed for the initial velocity profile. The similarity holds for general initial profiles provided the flow has the same initial profile as a function of y^*/δ_δ^*.

The present formulation is valid for shock waves of moderate strength, that is, for $\chi_t = 0(1)$. It is of interest to inquire into the behavior of the solutions in the limits of large and small values of χ_t. For $\chi_t = 0(1)$, the sonic line is in the main part of the defect layer and the appropriate length scales are the ones used in the present analysis. The sonic line approaches the wall for increasing values of χ_t and moves into the inner layers for large χ_t. In the large χ_t limit, it can be shown that the flow in the defect layer is described by a linearization about the piecewise constant normal-shock solution. A boundary-value problem similar to that treated by Adams[33] arises. This solution must develop a singularity at the wall. This suggests that the solution in the inner layer for large χ_t must be relatively complex and probably involves normal pressure gradients. An analysis of this problem has not yet been carried out.

For the weak shock limit of $\chi_t - 0$, the present formulation should reduce to that of Adamson and Feo.[21] This limit process, however, involves a complicated singular perturbation problem which is considered in Appendix B. There, we show that the present analysis includes the weak shock theory of Ref. 21.

V. Blending Layer

The structure of the solution in the two inner layers is such that the first two terms of the solution in the wall layer can be completely determined without consideration of the blending-layer solution. The first two terms in the skin friction can be obtained by comparing the wall-layer solu-

tion directly with the solution in the outer or defect region. In this way, it can be shown that the change in skin friction due to interaction with the shock wave is the order of the pressure rise, which, in the present problem is $0(\epsilon)$. Thus the shock strengths considered in the present investigation, $\chi_t = 0(1)$, are not large enough to cause separation.

Because of the freezing of the Reynolds stress in the outer layer, as discussed previously, the outer and wall layer regions do not overlap. Hence, to be logically consistent and to confirm the skin-friction solution, we should complete the wall-layer solution by matching to the solution in the blending layer. Therefore, in the present section, we will develop the asymptotic solution in the blending layer, carrying all terms that contribute to the second-order skin friction. For greater generality, we will retain all Mach number terms in these expansions and also in the wall layer. Transonic approximations consistent with the outer solution can then be obtained by expanding these solutions in powers of M_∞.

It is only at this stage of the analysis that empirical assumptions need be made in order to close the system of equations. Most of the correlations that appear in the time-averaged compressible flow equations vanish to the order required in the present study. Four assumptions must be made in order to close the blending-layer equations to second order. These are (1) an assumption relating turbulent kinetic energy to the Reynolds stress, (2) a model for the dissipation function, (3) an estimate of the pressure diffusion terms and (4) an estimate of the mean dilatation parameter α. In order to conveniently arrive at a definite set of equations, we will follow Bradshaw's[24,28] model of these terms. Thus, the pressure diffusion terms are asymptotically of higher order and do not appear in the second-order equations. This seems to be a reasonable approximation, since experimental data indicate that the pressure diffusion terms are much smaller than the other terms appearing in the turbulent kinetic-energy equation. In Bradshaw's model, the turbulent kinetic energy is assumed to be given by

$$e = \tau/2a_1\rho \tag{5.1}$$

where his suggested value of

$$a_1 = 0.15 \tag{5.2}$$

is most suitable for regions near the wall. The dissipation function is taken in the standard form,

$$\epsilon_d = \frac{(\tau/\rho)^{3/2}}{L_d(y)} \tag{5.3}$$

The dissipation length, $L_d(y)$, is assumed to have the following expansion

$$L_d(y) = \kappa y(1 + l_1 y + l_2 y^2 + \cdots) \tag{5.4}$$

where κ is the von Karman constant ($\kappa = 0.41$) and l_1, l_2 are constants that can be determined from a curve fit of Bradshaw's suggested function. The values of l_1, l_2 do not appear in the second-order equations and hence are not actually needed.

The requirement that the inertia and Reynolds stress terms in the streamwise momentum equations are of the same order leads to the lengths given in eqs. (2.9a) and (2.12). Using these length scales the following stretched variables are defined as

$$x^* = \epsilon^{1/2}\delta_0^* x \tag{5.5}$$

$$y^* = \epsilon^{3/2}\delta_0^* Y. \tag{5.6}$$

Preliminary analysis of the x momentum equation indicates that the first-order Reynolds stresses are balanced by the second-order inertia terms. This complicates the development of the solution, in that the expansion for u and p must be carried out to second order for a computation of the first term in the solution for the Reynolds stresses.

The expansion for u contains a number of $\log\epsilon$ terms that must be considered. These terms arise from contributions of the outer solution and from the initial profile. They can easily be extracted from these expansions when written in blending layer variables. Taking these terms into account and after some simple manipulations, the expansions for the blending layer solution can be written:

$$u = 1 + \left(\frac{3}{2\kappa}\right)\epsilon\log\epsilon - \epsilon^2(\log\epsilon)^2\left(\frac{3}{2\kappa}\right)^2\frac{m_s}{2} - \epsilon^2\log\epsilon\left(\frac{3}{2\kappa}\right)[m_s H(Y) - (1 + 2m_s)P_1(x)] + \epsilon^2 U_2(x, Y) + \cdots \tag{5.7}$$

$$v = \epsilon^2 V_1(x, Y) \tag{5.8}$$

$$p = 1 + \epsilon P_1(x) + \epsilon^2 P_2(x) + \cdots \tag{5.9}$$

$$\rho = 1 + \frac{3m_s}{\kappa}\epsilon\log\epsilon + \epsilon[2m_s H(Y) + M_\infty^2 P_1(x)] + \cdots \tag{5.10}$$

$$T = 1 - \left(\frac{3}{2\kappa}\right)(\gamma-1)\epsilon\log\epsilon + \epsilon(\gamma-1)[P_1(x) - H(Y)] + \cdots \quad (5.11)$$

$$\tau = \epsilon^2[1 + \epsilon\Gamma_1(x,Y) + 0(\epsilon^2\log\epsilon)] \quad (5.12)$$

$$e = \epsilon^2[2a_1 + \epsilon E_1(x,Y) + 0(\epsilon^2\log\epsilon)] \quad (5.13)$$

where

$$H(Y) = \frac{1}{\kappa}[\log Y - 2\bar{\pi}] . \quad (5.14)$$

Consideration of the normal momentum equation indicates that the pressure is constant across the blending layer to second order. Thus, the functions $P_1(x)$ and $P_2(x)$ appearing in eq. (5.9) can be determined from the wall values of the outer solution. Assuming that wall-layer displacement effects are negligible to second order, (as will be verified in the next section), we find from continuity considerations

$$V_1 = -(M_\infty^2 - 1)\frac{dP_1}{dx}\, Y. \quad (5.15)$$

In the transonic limit V_1 actually becomes first order in ϵ

$$V_1 = -\epsilon\chi_t \frac{dP_1}{dx}\, Y \quad \text{for } \chi_t = 0(1) . \quad (5.16)$$

Thus, the blending layer is a parallel stream to third order at transonic speeds.

Substitution of the previous expansion into the x momentum and turbulent kinetic-energy equations results in the following equations:

$$U_{2_x} - \Gamma_{1_Y} = -\frac{dP_2}{dx} + (1 + 2m_\infty)H(Y)\frac{dP_1}{dx} \quad (5.17)$$

$$\Gamma_{1_x} = 2a_1\left\{U_{2_Y} - \frac{\Gamma_1 - [M_\infty^2 P_1(x) + 2m_\infty H(Y)]}{2\kappa Y} - \alpha M_\infty^2 \frac{dP_1}{dx}\right\} \quad (5.18)$$

where the assumptions given in eqs. (5.1) through (5.4) were used to close the system of equations. We call attention to the fact that advection of turbulent kinetic energy is retained as a leading term and that convection is retained in the momentum equation. Thus, the shear stress gradient τ_y is not constant in this region. Hence, the blending layer is not a generalized equilibrium layer in the sense of Townsends theory[34] of turbulent separation.

The equations (5.17) and (5.18) can be somewhat simplified by the substitution

$$U_2 = U(x,Y) - P_2(x) + (1 + 2m_\infty)H(Y)P_1(x) + \tfrac{1}{2}m_\infty H^2(Y) \quad (5.19)$$

$$\Gamma_1 = \Gamma(x,Y) \quad (5.20)$$

whereby

$$U_x - \Gamma_Y = 0 \quad (5.21)$$

$$\Gamma_x - 2a_1 U_Y = -\frac{a_1}{\kappa Y}[\Gamma - \sigma P_1(x)] - 2a_1\alpha M_\infty^2 \frac{dP_1}{dx} \quad (5.22)$$

and where

$$\sigma = M_\infty^2 + 2(1 + 2m_\infty) . \quad (5.23)$$

Thus

$$\lim_{x\to-\infty} U(x,Y) = 0 \quad (5.24)$$

$$\lim_{x\to-\infty} \Gamma(x,Y) = 0 . \quad (5.25)$$

Homogeneous initial conditions are obtained because ϵ has been defined to be equal to the exact value of the skin friction at the initial station. Boundary conditions are determined by matching to the defect layer for $Y \to \infty$ and to the wall layer for $Y \to 0$. Matching to the defect layer leads to the condition

$$\lim_{Y\to\infty} U(x,Y) = 0 \quad (5.26)$$

In the following section, we show that the first order skin friction can be determined from the outer and wall-layer solutions independent of the blending-layer solution. This leads to the following inner condition:

$$\Gamma(x,0) = \tau_{1_w}(x) = -\beta P_1(x) \quad (5.27)$$

where P_1 is determined from solution to the outer problem and β is a constant determined from the wall layer solution.

The solution to the boundary value problem for $U(x,y)$ can be shown to have the following behavior for $y \to 0$

$$U = \tfrac{1}{2}[\tau_{1_w}(x) - \sigma P_1(x)][\log Y - 2\bar{\pi}] + C_2(x) \quad (5.28)$$

where $C_2(x)$ is a function that can be extracted from the numerical solution of the above problem. The function $C_2(x)$ is required in the wall-layer

solution to compute the second-order skin friction. Thus, the flow in the blending layer first affects the solution for the skin friction to second order. It follows that the effects of empirical closure approximation also enter only at this order.

Before leaving this section, we note that a compact statement of the blending-layer problem can be obtained by introducing a generalized potential, defined by

$$U = \Omega_Y \tag{5.29}$$

$$V = \Omega_x \ . \tag{5.30}$$

Equation (5.21) is automatically satisfied, and substitution into eq. (5.22) leads to the following second-order partial differential equation:

$$\Omega_{xx} - 2a_1\Omega_{YY} + \frac{a_1}{\kappa Y}\Omega_x = \frac{a_1 P_1(x)}{\kappa Y} - 2a_1\alpha\frac{dP_1}{dx}M_\infty^2 \ . \tag{5.31}$$

Equation (5.31) is a hyperbolic equation as must arise when the pressure diffusion terms are neglected (or approximated by Bradshaw's model). The last term in eqs. (5.18) and (5.31) arise from mean dilatation terms in the turbulent kinetic-energy equation. As noted by Bradshaw[26,27] and discussed previously, the values of α appearing in these terms must be carefully chosen to model the effects of extra mean dilatation. These terms are believed to have a value of about ten (Ref. 26) and therefore can be expected to have a larger effect on the skin friction than their formal magnitude (i.e., ϵ^2) would suggest. Considerations for determining values of α are given in Refs. 26 and 27.

VI. Wall Layer

In the wall layer, all correlations except the dissipation function are asymptotically negligible for the insulated flat plate under consideration. In our solution, we model the dissipation function in the usual manner by introducing a damping factor to account for viscous effects near the wall. Thus, we assume the dissipation is written in the form

$$\epsilon_d = \frac{(\tau/\rho)^{3/2}}{\kappa y D}$$

where D is the damping factor. There have been a number of choices for D, suggested in the literature. They are all equivalent if pressure gradients are not important in the wall layer, because then they are all based on the same set of zero pressure-gradient data. Although the pressure gradients in the present interaction problem are large, the shear stress gradients near the wall are even larger. An order of magnitude analysis of the momentum equation using the present length scales shows that the pressure gradient and inertia terms are exponentially small compared to the shear stress terms and hence can be neglected to all orders*. It follows that any of the standard zero pressure-gradient damping factors should be adequate for the present work. For example, Van Driest suggested the form

$$D = 1 - \exp(-y^*/26.) \tag{6.1}$$

where y^* is the local wall coordinate defined by

$$y^* = \left[\frac{\mu_w^*(x)}{\rho_w^*(x)u_\tau^*(x)}\right]y^* \tag{6.2}$$

The only property of D actually required in the present work is

$$\lim_{y^*\to\infty} D = 1 + \text{exponentially small terms} \tag{6.3}$$

The solution in the wall layer will be carried out in stretched coordinates x, y^*. We also introduce a wall layer velocity u^* by

$$u = u_\tau(x)u^* \tag{6.4}$$

We recall the definition of the local friction velocity

$$u_\tau = \sqrt{\frac{\tau_w(x;\epsilon)}{\rho_w(x;\epsilon)}} = O(\epsilon) \tag{6.5}$$

where $\rho_w(x;\epsilon)$ and $\tau_w(x;\epsilon)$ are the local wall density and local skin friction, respectively. Substitution of the above wall-layer variables into the governing equations and carrying out the limit $\epsilon \to 0$ (however, retaining all Mach number terms) and noting the order of magnitude estimate in eq. (6.5) we obtain

$$\frac{\tau}{\tau_w} + \frac{\mu}{\mu_w}\frac{\partial u^*}{\partial y^*} = 1 + O(\epsilon^3) \tag{6.6}$$

*As is well known[16],[19] this conclusion does not hold near separation. Hence the present developments are likely to be not uniformly valid near such points. An additional expansion, including pressure gradients, and a small length scale is probably required for this region.

$$\frac{\tau}{\tau_w} = \left(\frac{\rho}{\rho_w}\right)\left(\kappa y^* \frac{\partial u^*}{\partial y^*}\right)^2 D^2(y^*) + 0(\epsilon^3) \qquad (6.7)$$

$$\frac{\rho_w}{\rho} = 1 - a^2 u_\tau^2 (u^*)^2 \qquad (6.8)$$

$$\frac{\mu}{\mu_w} = K\left\{\frac{\rho_w}{\rho}\right\} \qquad (6.9)$$

$$v = 0(\text{exponentially small}) \qquad (6.10)$$

where $K\{\rho_w/\rho\}$ is defined from a specification of a particular viscosity model.

Equation (6.6) follows from the streamwise momentum equation. It is the usual condition that the total stress, laminar plus turbulent, is constant across the wall layer. Equation (6.7) is a mixing-length equation for the Reynolds stress, augumented by a damping factor to account for viscous effects on the length scale in the wall layer. In the present context it follows as a formal asymptotic consequence of the dominance of the production and dissipation terms in the turbulent kinetic-energy equation as $y \to 0$. We note that the mean dilatation terms are negligible to all orders in the wall layer. The density is computed from eq. (6.8) which follows from the equation of state and the condition that the pressure and total temperature are constant across the wall layer. The viscosity is computed from the density using an equation of the form given in eq. (6.9).

These are the usual equations used for incompressible and compressible wall layers. Inspection of the normal momentum equation indicates that pressure is constant across the wall layer to all orders. Thus, the pressure is imposed from the outer solution and is given the form

$$p = \frac{1}{\gamma M_\infty^2} + \epsilon p_{w_1}(x) + \epsilon^2 p_{w_2}(x) + \cdots \qquad (6.11)$$

Equation (6.10) indicates the v component of velocity is exponentially small. This implies that wall-layer displacement effects are negligible to all orders and that the normal velocity boundary conditions used in the outer regions are correct.

In order to develop wall-layer expansions that are valid in a region large enough to overlap the blending layer, we follow the procedures adopted in Section III for non-interacting boundary layers. Thus, we transform eqs. (6.6) through (6.8) using Van Driest's generalized velocities

$$u = u_\tau u^* = \frac{1}{a} \sin(a u_\tau \tilde{u}) \qquad (6.12)$$

We also define new dependent variables F, R in place of τ and ρ by the relations

$$\tau = \tau_w(x; \epsilon) F(x, y^*; \epsilon) = 0(\epsilon^3) \qquad (6.13)$$

$$\rho = \rho_w(x; \epsilon) R(x, y^*; \epsilon) = 0(1) \qquad (6.14)$$

where $\tau_w(x; \epsilon)$ is the order of the shear stress of the approaching boundary layer and is $0(\epsilon^2)$. Under these change of variables, the wall-layer equations become

$$F + [K(R)/R^{1/2}] \frac{\partial \tilde{u}}{\partial y^*} = 1 + 0(\epsilon^3) \qquad (6.15)$$

$$\sqrt{F} = D(y^*) \kappa y^* + \frac{\partial \tilde{u}}{\partial y^*} + 0(\epsilon^3) \qquad (6.16)$$

$$R = \frac{1}{\cos^2(a u_\tau \tilde{u})} \qquad (6.17)$$

with K(R) determined from a viscosity law.

Equations (6.15) to (6.17) are to be solved subject to the boundary condition

$$\tilde{u} = 0 \text{ for } y^* = 0 \qquad (6.18)$$

We note that the density appears only in the second term of eq. (6.15). This term is multiplied by a viscous term which becomes exponentially small in the fully turbulent part of the wall layer. As a result, the troublesome density terms cause no mathematical difficulties and we can represent the solution of the transformed equations in a limit-function expansion.

To solve the resulting equations, we must choose a particular model for the function $D(y^*)$ and for the viscosity law. The resulting equations for a given choice of $D(y^*)$ usually can only be integrated numerically. However, in order to match to the blending layer and to determine the skin friction, we only require a solution in the fully turbulent part of the wall layer. This is obtained in the usual fashion by dropping the viscous term in eq. (6.15), setting $D = 1$. The resulting equations reduce to the familiar incompressible form which can be integrated in closed form to yield

$$\tilde{u} = \frac{1}{\kappa} \log y^* + B(x; \epsilon) \qquad (6.19)$$

where $B(x; \epsilon)$ is a function that can only be determined from an integration of the full equations (i.e., eqs. (6.15) through (6.17)). Thus, $B(x; \epsilon)$ must depend upon the density variations through

the second term in eq. (6.15). Noting that $u_\tau = 0(\epsilon)$, eq. (6.17) indicates that B must be of the form

$$B = B_0 + \epsilon^2 B_2(x) + \cdots \tag{6.20}$$

where the first term can be identified with the incompressible value and the second term contains the first effects of compressibility in the wall layer (in transformed variables). The incompressible constant B_0 is a function of the damping model employed in the computations. These models are usually arranged to give the experimentally accepted value of $B_0 = 5.0$.

Thus, the solution in the fully turbulent part of the wall layer can be written as

$$u = \frac{1}{a}\sin\left\{\epsilon a\sqrt{\frac{\tau_w(x;\epsilon)}{\rho_w(x;\epsilon)}}\left[\frac{1}{\kappa}\log y^* + B_0 + \epsilon^2 B_2 + \cdots\right]\right\} \tag{6.21}$$

The wall density can be related to the surface pressure through the equation of state evaluated at the constant wall temperature. The skin friction is an arbitrary function of x and ϵ at this stage of the analysis. It will eventually be determined by matching the wall and blending-layer solutions. Matching considerations suggest that τ_w and ρ_w can be expanded as

$$\tau_w = \epsilon^2[1 + \epsilon\tau_{w_1} + \epsilon^2\log\epsilon\,\tau_{w_{21}} + \epsilon^2\tau_{w_{22}} + \cdots] \tag{6.22}$$

$$\rho_w = \rho_{w_0} + \epsilon\rho_{w_1} + \epsilon^2\rho_{w_2} + \cdots \tag{6.23}$$

From the equation of state we find

$$\rho_{w_0} = 1 - a^2 \tag{6.24}$$

$$\rho_{w_1} = \gamma M_\infty^2 p_{w_1}(x) \tag{6.25}$$

$$\rho_{w_2} = \gamma M_\infty^2 p_{w_2}(x) \tag{6.26}$$

The first term above, is the wall density in the non-interacting flow upstream of the shock wave. With these results the wall-layer solution for the velocity can be written as

$$u = \frac{1}{a}\sin\left(\frac{\epsilon a}{\sqrt{\rho_{w_0}}}\left\{\left[\frac{1}{\kappa}\log y^* + B_0\right] + \tfrac{1}{2}\epsilon[\tau_{w_1} - \rho_{w_1}]\frac{1}{\kappa}\log y^* + \tfrac{1}{2}\epsilon^2\log\epsilon[\tau_{w_{21}}]\frac{1}{\kappa}\log y^* + \tfrac{1}{2}\epsilon^2[\tau_{w_{22}} - \rho_{w_{22}} + 2\rho_{w_1}^2 - \tfrac{1}{4}(\tau_{w_1} - \rho_{w_1})^2 + 2B_2] + \cdots\right\}\right) \tag{6.27}$$

Notice that the solution for u is not in the form of a limit-function expansion. If the above expression is further expanded into limit-function form, it can be shown that the resulting solution will not match with the blending-layer solution. The demonstration that the generalized wall-layer solution given above can be matched term by term to the blending-layer solution is somewhat involved, and the details are given in Appendix C. Here, we present the solution for the skin friction to second order which comes from the requirement that wall and blending-layer solutions match to second order

$$\frac{C_f}{C_{f_0}} = 1 + \epsilon\left[\gamma M_\infty^2 - \frac{2}{q}\right]p_{w_1} + 3\epsilon^2\log\epsilon\left[\frac{1 + (1 + m_\infty)q}{q^2\kappa}\right]p_{w_1} + \epsilon^2\left[\left(\gamma M_\infty^2 - \frac{2}{q}\right)p_{w_2} - \left(\gamma^2 M_\infty^4 - \frac{1 + m_\infty q}{q^2}\right) \times p_{w_1}^2 - \frac{2B_0}{q^2}p_{w_1} + \frac{2C_2}{q}\right] \tag{6.28}$$

where

$$q = \sqrt{\rho_{w_0}}\,\tilde{u}_e = \sqrt{\frac{1 - a^2}{a^2}}\,\sin^{-1}a\,. \tag{6.29}$$

The evaluation of the second-order skin friction from the above expression requires a numerical solution of the boundary-value problem formulated in the blending layer in order to determine the function $C_2(x)$, appearing in eq. (6.28). The transonic limit of eq. (6.28) is obtained by setting M_∞ to one in the above expression. For reference, we note

$$\left.\begin{aligned} a &= 0.40825 \\ \sigma &= 0.94034 \end{aligned}\right\} \text{ for } M_\infty = 1.$$

VII. Numerical Analysis of the Outer-Layer Equations

This section presents the numerical analysis of the first-order ($\ln\epsilon$) outer-layer equations and boundary conditions as described by eqs. (4.14)–(4.19). As shown in Sections V and VI, normal pressure gradients in the wall and blending layers are zero to second order. Thus, the solution of the above outer-layer equations will trace the development of the pressure distribution from a discontinuous jump at the normal shock to a smooth rise at the surface. This surface pressure distribution can then be used to solve the blending and wall layers for the skin friction.

The complete boundary-value problem is restated here as

$$(\gamma + 1)[\lambda(y) - \phi_x]\phi_{xx} + \phi_{yy} = 0 \tag{7.1}$$

with

$$\lambda(y) = -\left[\frac{\chi_1}{\gamma+1} + u_1(y)\right] \tag{7.2}$$

and

$$\lim_{y\to\infty} \phi_x(x,y) = \begin{cases} 0\ , & x<0 \\ 2\lambda_\infty, & x>0 \end{cases} \tag{7.3}$$

$$\lim_{x\to-\infty} \phi_x(x,y) = 0 \tag{7.4}$$

$$\lim_{x\to+\infty} \phi_x(x,y) = 2\lambda_\infty \tag{7.5}$$

and at the surface

$$\phi_y(x,0) = 0 \tag{7.6}$$

with

$$\lambda_\infty = -\chi_1/\gamma+1$$

The only quantities remaining to complete the boundary-value formulation is the oncoming boundary-layer defect profile $u_1(y)$. In principle, this profile may be obtained from experimental data. However, consistent with the formalism used to develop the analysis in the inner layers, we describe $u_1(y)$ as the non-interacting boundary layer profile given by eq. (3.13). Hence, the boundary-value problem as described by eqs. (7.1)–(7.6) will possess a two-parameter family of solutions, depending on values of the interaction parameter χ_1 and the initial profile shape factor $\bar{H}$.

One difficulty with the above formulation lies in the implementation of the surface boundary condition, eq. (7.6). Standard numerical techniques evaluate this condition through a reflection plane procedure, which requires the governing eq. (7.1) to be evaluated at the wall $y = 0$. However, due to the logarithmic behavior of the initial profile $u_1(y)$, the coefficient $\lambda(y)$ becomes singular for $y \to 0$.

One way of circumventing this problem is to expand $\lambda(y)$ for small y as

$$\lambda(y) = b_0 \log y + b_1 + O(y^2) \tag{7.7}$$

where b_0 and b_1 are known constants. The behavior of ϕ near the wall can be seen to be of the form

$$\phi(x,y) = \phi(x,0) + c_1(x)y^2 \log y + c_2(x)y^2 + O(y^3)\ . \tag{7.8}$$

Inserting eqs. (7.7) and (7.8) into (7.1), retaining lowest-order terms and comparing similar terms in y gives

$$c_1(x) = -\frac{(\gamma+1)}{2} b_0 \phi_{xx}(x,0) \tag{7.9}$$

and

$$c_2(x) = -\frac{(\gamma+1)}{2}\left[b_1 - \tfrac{3}{2}b_0 - \phi_x(x,0)\right]\phi_{xx}(x,0)\ . \tag{7.9}$$

Now, eq. (7.8) may be solved for $\phi(x,0)$ in terms of the solution at a small distance y away from the wall, with the terms c_1 and c_2 obtained from eq. (7.9) involving x-derivatives of the wall solution from a previous iterate.

The above boundary-value representation is still not in a form suitable for numerical integration. The tangential boundary conditions at the shock, eq. (7.3) must be replaced by the appropriate Dirichlet condition. Without loss in generality, this is accomplished by

$$\lim_{y\to\infty} \phi(x,y) = \begin{cases} 0\ , & x<0 \\ 2\lambda_\infty x, & x>0 \end{cases} \tag{7.10}$$

But, eq. (7.10) introduces another numerical difficulty. The limit of $\phi(x,y) = 2\lambda_\infty x$ as $y \to \infty$ cannot be applied as $x \to \infty$. We have chosen to solve this problem by separating the infinite domain into two parts. Part 1, $x < 0$, we have

$$\phi_1 = \phi \qquad \lim_{y\to\infty} \phi_1(x,y) = 0$$
$$\lim_{x\to-\infty} \phi_1(x,y) = 0, \qquad \phi_{1_y}(x,0) = 0 \tag{7.11}$$

And, for part 2, $x > 0$, we have

$$\phi_2 = \phi - 2\lambda_\infty x\ , \qquad \lim_{y\to\infty} \phi_2(x,y) = 0$$
$$\lim_{x\to\infty} \phi_2(x,y) = 0, \qquad \phi_{2_y}(x,0) = 0 \tag{7.12}$$

The interface equations across the boundary $x = 0$ are

$$\phi_1(0,y) = \phi_2(0,y)$$
$$\phi_{1_x}(0,y) = \phi_{2_x}(0,y) + 2\lambda_\infty \tag{7.13}$$

The equation governing ϕ_1, is identical to equation (7.1) replacing ϕ by ϕ_1. The equation for ϕ_2 is written as

$$(\gamma+1)[\lambda(y)-2\lambda_\infty-\phi_{\xi\xi}]\phi_{\xi\xi}+\phi_{\eta\eta}=0 \quad (7.14)$$

This formulation is illustrated in Fig. 3.

In order to develop a domain suitable for the numerical solution of the above equations, we analytically transform the upper half plane (physical domain) to a unit square (computational domain). The particular functions are chosen to be

$$x=\begin{cases}\left(A_1+A_2\log\dfrac{\xi}{\xi_A}\right)\log\dfrac{\xi}{\xi_A}+A_3\xi_A+A_4, & \xi<\xi_A\\ A_3\xi+A_4, & \xi_A\le\xi\le\xi_B\\ \left(A_5+A_6\log\dfrac{1-\xi}{1-\xi_B}\right)\log\dfrac{1-\xi}{1-\xi_B}+A_3\xi_B+A_4, & \xi>\xi_B\end{cases} \quad (7.15)$$

and

$$y=\begin{cases}A_7\,\eta, & 0\le\eta\le\eta_A\\ \left(A_8+A_9\log\dfrac{1-\eta}{1-\eta_A}\right)\log\dfrac{1-\eta}{1-\eta_A}+A_7\eta_A, & \eta>\eta_A\end{cases} \quad (7.16)$$

The above functions are seen to have the appropriate behavior since $\xi(-\infty)=0$, $\xi(+\infty)=0$, $\eta(0)=0$ and $\eta(\infty)=1$. Furthermore, constant rectangular mesh spacings $\Delta\xi$, $\Delta\eta$ in the computational domain yield the variable mesh in the physical plane as depicted in Fig. 4. The stretching functions (7.15) and (7.16) are chosen to have a uniform grid in the physical plane within a rectangular region surrounding the shock, near the surface. The mesh lines then expand nonuniformly to infinity in all directions. The parameters A_1-A_9, ξ_A, ξ_B and η_A are used to determine the size of the mesh in the inner rectangular region and to control the rate of this mesh growth to infinity. The transformations were chosen with this uniform inner rectangular grid in order to carefully study the region where the shock meets the outer edge of the boundary layer with minimal effects of variable mesh spacing. The derivatives of the transformation are used in the solution of eqs. (7.1) and (7.14) as

$$\phi_x=\phi_\xi\xi_x \qquad \phi_y=\phi_\eta\eta_y$$
$$\phi_{yy}=\phi_\xi\xi_{yy}+\phi_{\xi\xi}\xi_y^2 \quad \phi_{yy}=\phi_\eta\eta_{yy}+\phi_{\eta\eta}\eta_y^2 \quad (7.17)$$

It has recently been found that an efficient and accurate means of solving this system consists of a mixed flow line-relaxation procedure introduced by Murman and Cole.[20] This technique has been successfully applied to a variety of inviscid transonic aerodynamic problems and to the computation of a discontinuous wave near a caustic.[35] This latter problem results in a somewhat similar equation to eq. (7.1) with λ being proportional to y.

A line-relaxation algorithm is developed to solve the outer problem. A uniform rectangular grid is employed in the computational plane with mesh spacings $\Delta\eta$ and $\Delta\xi$. Subscripts N and M in the following analysis refer to the counters respectively locating the ξ and η mesh lines. For regions of subsonic flow, the following difference expressions are used

$$\phi_\xi=\frac{\phi^\nu_{N+1,M}-\phi^\nu_{N-1,M}}{2\Delta\xi} \quad (7.18)$$

$$\phi_{\xi\xi}=\frac{\phi^\nu_{N+1,M}-\frac{2}{\omega}\phi^{\nu+1}_{N,M}+\frac{2}{\omega}(1-\omega)\phi^\nu_{N,M}+\phi^{\nu+1}_{N-1,M}}{\Delta\xi^2} \quad (7.19)$$

where the superscript ν refers to values at the previous iterate and $\nu+1$ refers to the present iterate. The quantity ω is the relaxation factor which on the basis of linearized stability considerations lies between 0 and 2. For this study, we take $\omega>1$ corresponding to over-relaxation.

In regions of supersonic flow, we take

$$\phi_\xi=\frac{\phi^{\nu+1}_{N,M}-\phi^{\nu+1}_{N-2,M}}{2\Delta\xi} \quad (7.20)$$

$$\phi_{\xi\xi}=\frac{\phi^{\nu+1}_{N,M}-2\phi^{\nu+1}_{N-1,M}+\phi^{\nu+1}_{N-2,M}}{\Delta\xi^2}, \quad (7.21)$$

and for both regions we take

$$\phi_\eta=\frac{\phi^\nu_{N,M+1}-\phi^\nu_{N,M-1}}{2\Delta\eta} \quad (7.22)$$

$$\phi_{\eta\eta}=\frac{\phi^{\nu+1}_{N,M-1}-2\phi^{\nu+1}_{N,M}+\phi^{\nu+1}_{N,M-1}}{\Delta\eta^2}. \quad (7.23)$$

In order to determine whether the flow is supersonic, the following test function is used

$$\phi_{\xi test}=\frac{\phi^\nu_{N,M}-\phi^\nu_{N-2,M}}{2\Delta\xi} \quad (7.24)$$

and the supersonic differencing procedure is used when

$$\xi_x\phi_{\xi test}-\lambda(y)>0 \quad (7.25)$$

This particular test function has been found to be stable for purely decelerating flows. In addition,

we have found that for the present problem, this choice of test function results in shocks smeared over a minimum number of mesh intervals (i.e. 1-2).

The above difference formulae, (7.18)–(7.24), are arranged using standard methods in a convenient algorithm to update values of ϕ in successive columns starting with $\xi = 0$ proceeding to $\xi = 1$. Note that with the above schemes, the difference equations will be non-linear in supersonic regions due to the presence of $(\phi^{\nu+1}_{M,M})^2$ terms. This requires a local fixed-point iteration as discussed in Ref. 20.

It is seen from eqs. (7.4) and (7.5) that the value of $\phi_x - 2\lambda_\infty = -2\chi_t/\gamma+1$ as $x \to +\infty$. In order to compare runs at different values of χ_t, we found it convenient to introduce following additional transformations:

$$\bar{x} = x/\sqrt{\chi_t} \tag{7.26}$$

and

$$\bar{\phi} = (\gamma+1)\,\phi/\chi_t^{3/2}, \tag{7.27}$$

whereby equations (7.1) and (7.2) become

$$[\bar{\lambda}(y) - \bar{\phi}_{\bar{x}}]\bar{\phi}_{\bar{x}\bar{x}} + \bar{\phi}_{yy} = 0 \tag{7.28}$$

and

$$\bar{\lambda}(y) = -\left[1 + \frac{(\gamma+1)}{\chi_t}\,u_t(y)\right].$$

Now, we see that $\bar{\phi}_{\bar{x}} \to -2$ as $\bar{x} \to \infty$. Note that in terms of physical variables

$$\frac{x^*}{\delta_0^*} = \epsilon^{1/2} x = \sqrt{\epsilon\chi_t}\;\bar{x} = \sqrt{M_\infty^2 - 1}\;\bar{x} \tag{7.29}$$

We note for reference, that eq. (7.28) possesses real characteristics upstream of the shock wave and above the sonic line of the oncoming boundary layer. The characteristic directions are

$$\frac{dy}{d\bar{x}} = \pm\,\frac{1}{\sqrt{\bar{\phi}_{\bar{x}} - \bar{\lambda}}} \tag{7.30}$$

We also define a normalized perturbation pressure

$$\bar{p} = -\bar{\phi}_{\bar{x}} = -\frac{(\gamma+1)}{\chi_t}\,\phi_x = \frac{\gamma+1}{\chi_t}\,p_1 \tag{7.31}$$

which will be used in the next section where the numerical results will be discussed.

VIII. Results

The results of the numerical computation of the first-order, outer-layer equation are presented. As we have previously stated, the solution of this problem depends only on the value of the interaction parameter χ_t and the initial profile shape factor $\bar{n}$.

The first case considered is for $\chi_t = 7.5$ and $\bar{n} = 0.5$. Figure 5 indicates the calculated shock shape and sonic line. We note that upstream of the interaction, the sonic line appears near the middle of the boundary layer. In addition, in the supersonic flow ahead of the shock and outside the boundary layer, the flow is a simple wave type. Using the computed values of $\phi_{\bar{x}}$ along the line $y^*/\delta^* = 1$, we have traced the characteristic waves using eq. (7.30). It is seen that these compression waves emanating from the curved sonic line within the boundary layer, intersect the impinging normal shock causing it to bend forward. Although the characteristics tend to merge together near the shock, there is no evidence of shock focusing to form another leg of the shock pattern. Also, the shock blends smoothly into the sonic line within the boundary layer. The distributions of the normalized perturbation pressure $\bar{p}$ defined in eq. (7.31) are plotted vs $\bar{x}$ for several values of y, as shown in Fig. 6. This figure gives an indication of how the pressure transforms from a discontinuous jump far from the wall to a smooth pressure rise at the surface. Comparison of the distributions at $y = 0, 0.5$, and 1 illustrate the small, but significant effect of the normal pressure gradient through the boundary layer. For larger values of y, the pressure steepens to a shock wave and eventually overshoots the undisturbed value at $y = 4.5$. For succeedingly larger values of y the pressure overshoot decays to the normal shock value. The general features of the pressure distribution, including the overshoots are in qualitative agreement with the measurements of Gadd, [30] for a case with nearly the same values of χ_t and $\bar{n}$. However, we note that the overshoots in Gadd's data are at least partially due to an axial pressure gradient induced by wall effects downstream of the shock wave. Another feature of this calculation is shown in Fig. 7. Here the normalized velocity profile $u^*/u^*_\infty = 1 + \epsilon(u_1 + \phi_x)$ with $\epsilon = 0.034$ is plotted vs y for several values of x. The figure shows the velocity profile proceeding from the Coles' law of the wall-law of the wake form at upstream infinity, to the same profile uniformly decreased by the normal shock values far downstream. The intermediate profiles show the transition between the two extremes, with a smooth

transition occurring near the wall and an abrupt change far from the wall. The velocity at $x = -0.5$ shows the profile through the curved shock, which it intersects at approximately $y = 2.5$. Although it is not very pronounced in the figure, the velocity profiles exhibit overshoots down-stream of the interaction at several boundary thickness above the plate. Overshoots of this type have been noticed in experiments on shock wave-boundary layer interactions (c.f. Vidal et al[37]).

The flow-field structure discussed for this first case is typical of others where our analysis is applicable. To indicate the effect of χ_t on our solution, we computed results at $\chi_t = 5, 7.5, 10, 20,$ and 40, all with $\bar{\pi} = 0.5$. Figure 8 indicates the effect of χ_t on the normalized surface perturbation pressure distribution vs x. We see that in this coordinate system, the pressure rise steepens for increasing χ_t and the pressure distribution becomes only slightly more asymmetrical with respect to the incident shock position ($x = 0$). In the original coordinate, $x = \sqrt{\chi_t}\,\bar{x}$, the scale of the interaction is magnified and the asymmetry of the pressure distribution becomes somewhat more pronounced. However, we do not see the development of a long tail down stream of the shock, as will be discussed later.

Fig. 9 indicates the variation of the shock wave and sonic line as a function of χ_t. We see that as the interaction parameter increases, the sonic line approaches the wall. Also, in this limit, the results show the shock wave becoming more normal and penetrating further into the boundary layer.

The effect of $\bar{\pi}$ on the initial boundary-layer defect profile is shown in Fig. 10. Decreasing $\bar{\pi}$ results in a more "full" velocity profile. These profiles were then used to compute a set of outer-layer solutions at $\chi_t = 20$. From Fig. 11, we see that decreasing $\bar{\pi}$ to achieve fuller initial profiles results in steeper surface pressure gradients.

Next, we illustrate our numerical solution in comparison with the free interaction solution of Adamson and Feo[21] (eq. (B.11)). Here, we plot their result in terms of our variables $\bar{p}$ and $\bar{x}$ for the case $\chi_t = 7.5$. Their solution, however, only gives a surface pressure distribution up to sonic, and contains an arbitrary additive constant to the value of $\bar{x}$. Thus, to compare it to our solution, we had to superimpose Adamson and Feo's result and attempt to match the pressures. But, comparing to our surface pressure, the agreement was not very good. However, since their analysis neglected normal pressure gradients through the boundary layer, we felt it to be more applicable to compare to our results at the edge of the boundary layer, $y = 1$. The comparison shown in Fig. 12 is seen to be quite good and substantiates the agreement between the two theories for small χ_t.

Next, we attempted to compare our calculation with experimental data. We had to restrict ourselves to normal shock data from a high Reynolds number facility, with a fully developed, non-separated, turbulent boundary layer, for which $\chi_t = O(1)$. The experiments which came nearest to fitting these requirements were those of Gadd.[36] His experiments included a case where $M_\infty = 1.12$, $\epsilon = 0.0339$ and $\chi_t = 7.502$. Unfortunately, the test took place in a relative small diameter circular tube with strong axial pressure gradients. His post shock data never reached the inviscid shock jump, even at large distances away from the wall. Nevertheless, we present a comparison of our calculation with his result in Fig. 13. Here the notation p^*/p_0^* corresponds to the ratio of static pressure to the stagnation pressure upstream of the interaction. We see that the numerical and experimental results show similar overall trends.

The recent experimental data of Vidal et al,[37] were taken in a Ludwieg tube at very high Reynolds number, $Re = 36 \times 10^6$. Unfortunately, their runs were at $M_\infty = 1.4$ and $\epsilon = 0.024$ with $\chi_t = 40.5$ and contained a separation bubble. The pressure seemed to have an upstream influence of 1-2 boundary-layer thickness followed by a very long tail, (greater than ten boundary-layer thickness) where it slowly rises towards the normal shock value. The Mach number for this case is relatively high, necessitating the use of the extended small disturbance theory (i.e., eq. (4.27)). In addition, the data shows evidence of a weak disturbance upstream of the main interaction. The effect of this disturbance can be taken as a lowering of the interaction Mach number. Hence, for our calculation we used a value of $M_\infty = 1.32$ instead of 1.4, for which the similarity parameter $\bar{K}_t = 7.5$. Again, the numerical and experimental results show reasonable qualitative agreement. The scale of the upstream influence is approximately the same, but the downstream scales are not in agreement. We note that this calculation, using the extended theory, recovered the exact pressure jump across a normal shock, whereas the experiment showed an extremely slow approach towards the normal shock value.

Before proceeding with a discussion of these results in the next section, we will give some details of the numerical calculations. All runs con-

sidered here contained 78 mesh points in the ξ direction and 57 in the η direction. The last mesh point before infinity in the physical plane was at $x = \pm 20$ and $y = 20$. Typically 16 points were included within the boundary layer $0 < y < 1$ with a similar mesh in the inner rectangle (see Fig. 4) in the x direction. The solutions converge to a maximum residual of 10^{-5} in 100 - 800 iterations with the lower value corresponding to $\chi_t = 40$ and the higher value to $\chi_t = 5$. The corresponding computation times were from 1 to 6 minutes on an IBM 370/168. A relaxation factor $\omega = 1.75$ was used for the subsonic region and $\omega = 1.0$ for the supersonic region. A numerical stability problem was encountered for values of $\chi_t < 5$, for which we could not obtain any converged results. Another difficulty encountered was the use of the wall boundary condition, eq. (7.9). This condition was apparently unstable and we had to resort to the original wall condition eq. (7.6). We circumvented the logarithmic singularity in $\lambda(y)$ by considering the wall to be located at $y = 10^{-5}$ instead of at zero. Numerical studies varying this small wall displacement showed negligible effects on the calculated surface pressures. Various studies also were made on the effect of mesh size and mesh distribution on the accuracy and stability of the method. To illustrate just one of these results, we present in Fig. 15 two calculations for $\chi_t = 10$, $\bar{\pi} = 0.5$ computed with 8 and 16 points in the boundary layer.

IX. Discussion

Our objective has been to develop a rational approach for analyzing the interaction of shock waves with turbulent boundary layers. The present analysis considered the interaction involving weak normal shock waves and fully developed turbulent boundary layers. Under these conditions, the sonic line is located in the main part of the approaching boundary layer and as a result the surface pressure rises more smoothly than in interactions at higher Mach numbers. We have developed a complete asymptotic theory for this type of interaction in the double limit of large Reynolds numbers and Mach numbers approaching one.

The asymptotic structure has been shown to involve three layers and we have determined the leading terms of the solution in each region. The three-layer structure is numerically significant, since the middle or blending layer contributes logarithmic terms to the skin friction solution that are multiplied by relatively large constants (i.e., $3/\kappa \approx 7.3$). One of the unexpected findings of the present study was the discovery that the method of matched asymptotic expansions fails for compressible turbulent boundary layers. We have shown that transformation to Van Driest's generalized velocities circumvents this difficulty and enables us to obtain complete solutions in the inner layers.

The asymptotic theory for the outer region leads to a similarity parameter, $\bar{K}_t$, which is proportional to the ratio of the velocity change across the shock wave to the velocity defect in the upstream boundary-layer profile. Examination of the outer equations indicates that the solution depends upon the value of two parameters $\bar{K}_t$ and $\bar{\pi}$ where $\bar{\pi}$ is a measure of the profile shape in Coles' correlations. The value of the Reynolds number and Mach number influence the solution only through their effect on $\bar{K}_t\{M_\infty, \epsilon\}$. Thus, a similarity exists for moderate strength interactions ($\bar{K}_t = O(1)$).

We have demonstrated that our analysis for moderate shock strengths reduces to Adamson and Feo's,[21] theory as the shock strength approaches zero. A numerical comparison has indicated that the theories are in good agreement for χ_t as large as 7.5 (or $\bar{K}_t = 2.125$). Our results for this case, given in Fig. 12, show a significant pressure variation through the boundary layer, particularly near the shock wave. This pressure variation is an important feature of the flow in the region where the shock wave penetrates into the boundary layer. Nevertheless, it is interesting that Adamson and Feo's free interaction solution is apparently quite accurate over the entire supersonic region, when assumed to apply at the edge of the boundary layer, rather than at the wall.

We have implemented a mixed-flow relaxation technique for solving the inviscid outer-flow problem and have presented results for various values of χ_t between 5 and 40. Numerical convergence problems prevented us from obtaining solutions for values of χ_t less than 5. Our results give a reasonably complete picture of the structure of the wave pattern in a turbulent shock wave interaction. The present solution and the free-interaction solution of Ref. 21 indicate that the development of embedded shock waves by focusing of compression waves in the upstream flow does not occur. Rather, the wave pattern appears to develop by the simple mechanism of compression waves being generated by thickening of the subsonic part of the boundary layer and then intersecting the approaching shock wave and causing it to bend forward. The numerical results seem to indicate that the shock continues to

bend forward until it joins smoothly to the sonic line in the boundary layer. Variation in the parameters χ_t and $\bar{\gamma}$ have little effect on the general structure of the wave pattern. However the value of χ_{t_c}, does have a strong influence on the scale of the wave pattern. As χ_t increases the sonic line approaches the wall, and the shock wave becomes more normal with most of the interaction occurring near the impingement point of the undisturbed shock wave.

Experiments with normal shock waves sometimes indicate the presence of a supersonic tongue and a second (bifurcated) shock wave with the overall shock structure resembling a Mach reflection. A supersonic tongue is evident in Seddon's[38] data, but not in the data of Vidal et al. [37] The present numerical results do not show the existence of either a supersonic tongue or a second (bifurcated) shock wave. The reasons for the absence of these features in the present calculation are not clear. It may be that these effects are present only for strong shock waves involving separation and hence are not covered by the simple theory developed here. It is also possible that the present numerical scheme is not accurate enough to resolve the fine details of the flow near the shock impingement point. A finer mesh and a more accurate finite-difference method than the first-order scheme, used for supersonic points in the present calculation, may be required for this purpose. In any event, the present results indicate that the wave pattern is not a Mach reflection in the usual sense of the term. The "forward limb," described in experimental results is shown to be a simple continuation of the main shock wave. The "rear limb", when it is present, is just a simple recompression of the flow in a supersonic tongue to subsonic speeds. There does not seem to be any reason for assuming that the "rear limb" must intersect the main branch of the shock wave to form a triangular shock pattern.

As a final remark on flow structure, we note that the streamwise length scale exhibits a minimum as a function of χ_t. The minimum length scale occurs for $\chi_t = O(1)$ and increases in both limits of χ_t large and small. For large χ_t the increase in length is strongly asymmetrical with the interaction distance increasing on the downstream side of the shock wave and becoming vanishingly small on the upstream side.

The present theory indicates that the surface pressure distribution is relatively diffuse and nearly symmetrical for moderate to weak shock strengths, $\chi_t < 10$ and becomes more one-sided and steep on the upstream side for strong shocks, $\chi_t > 20$. Although this general trend is in accord with experimental observations, the theoretical calculations do not show the very long tail characteristic of surface pressures measured behind normal shock waves in wind tunnel experiments.[36–38]

In these experiments, the pressure distributions downstream of the shock wave showed little indication of approaching the normal shock limit over the region surveyed by the experiment. In Refs. 36 and 37 the pressure was measured to about $10\,\delta_0^*$ behind the shock wave and in Ref. 38 the downstream extent was about $50\,\delta_0^*$. The underlying cause of these long pressure "tails" most likely stems from wall or other interference effects in the subsonic flow downstream of the shock wave. This was definitely a factor in the measurements of Gadd. [36] He called attention to the presence of significant axial pressure gradients in the downstream flow and suggested that they were due to displacement effects induced by the wall boundary layers. The experiments of Seddon[38] and Vidal et al[37] contained regions of separated flow. The presence of these separation bubbles could have a large effect on the downstream flow and be a factor in the formation of pressure tails. Clearly, further experimental and theoretical efforts are necessary to understand the reasons for the disparity in the downstream results. However, because of the large region of subsonic flow behind the shock wave, it may be very difficult to eliminate or correct the data for wall interference in experiments on normal shock waves in wind tunnels.

We have developed a solution for the leading terms of the skin friction in terms of the outer-layer wall pressure distribution. Preliminary comparison with data (not presented here) indicates that this solution is not accurate for transonic Mach numbers. The difficulty appears to be associated with the anomalous mean dilatation effects, that Bradshaw[26] has shown to be important in compressible boundary layers with pressure gradients.

Although the skin friction is not accurate, it can be used as a guide to estimate the incipient separation pressure rise. The skin friction solution indicates that the change in skin friction is proportional to the change in surface pressure. Thus, the pressure rise required to separate a turbulent boundary layer is O(1), that is, independent of Reynolds number in the limit of large Reynolds number. This conclusion, which was also arrived at by Adamson and Feo, [21] is in broad

agreement with the high Reynolds number data of Roskho and Thomke.[11] It is interesting that Townsend[34] reached this conclusion a decade ago in his studies of turbulent separation in low speed flows.

The present results represent the first step in the development of more complete theory of the interaction of shock waves with turbulent boundary layers. The results suggest the following problems that appear worthwhile for future study.

- The extension of the present theory to strong shock waves with pressure rises of 0(1). Our results indicate that this is the range of shock strength that is important for practical problems involving separation.
- The development of higher-order terms in the outer expansions. This extension should be carried with a view to explaining the absence of the long pressure tails in the present theory. The understanding of the pressure tails is essential for improving the agreement between theory and experiment. In this regard it would be very useful to carry out careful experiments for interactions with shock waves of moderate strength over a range of χ_t of less than 10. High Reynolds numbers are not essential for this purpose. However special care should be exercised to determine the effect of tunnel interference on the development of the pressure tails.
- There is a need to improve the solution for the skin friction. The present results indicate that the effects of anomalous mean dilatation are important and need careful consideration.
- The numerical algorithm used in the outer region should be improved to include a more satisfying implementation of the wall boundary condition and to obtain greater accuracy in the supersonic region. There is a need to develop a second-order accurate finite-difference scheme for supersonic points in a mixed flow relaxation procedure. This would allow greater resolution near the shock impingement point and enable a more careful study of "supersonic tongues" and the second shock wave. It would also be useful to uncover the reasons for the lack of convergence of the iterative solution for small χ_t, ($\chi_t < 5$).
- The present theory is applicable only to flat surfaces. The effects of even a small amount of curvature are known to be significant. Inviscid theory indicates the presence of a strong, singular expansion just downstream of a normal shock wave on a curved surface. Experiments on airfoils indicate that the pressure behind the shock wave differs from the normal shock pressure determined from the shock jump conditions. The data shows that pressure behind the shock wave is usually quite close to sonic, independent of shock strength. The reasons for this are unknown, although it is clear that it must be related to a complex interplay between the inviscid expansion and the shock wave-boundary layer interaction process. Thus it is clear that the present theory must be extended to include surface curvature effects if it is to apply to interactions of practical importance.

REFERENCES

1. Green, J. E., "Interactions Between Shock Waves and Turbulent Boundary Layers", article in Progress in Aeronautical Sciences, Vol. 11, Pergamon Press, 1970.
2. Lighthill, M. J., "On Boundary Layers and Upstream Influence. II, Supersonic Flows Without Separation", Proc. Roy. Soc., Series A, Vol. 217, 1953.
3. Howarth, L., "The Propagation of Steady Disturbances in a Supersonic Stream Bounded on One Side by a Parallel Subsonic Stream", Proc. Cambridge Philos. Soc., Vol. 44, 1948.
4. Tsien, H. S. and Finston, M., "Interaction Between Parallel Streams of Subsonic and Supersonic Velocities", J. Aero. Sci., Vol. 16, No. 9, 1949.
5. Stewartson, K., "On the Flow Near the Trailing Edge of a Flat Plate. II", Mathematika, Vol. 16, 1969.
6. Messiter, A. F., "Boundary-Layer Flow Near the Trailing Edge of a Flat Plate", SIAM J. Appl. Math., Vol. 18, No. 1, Jan. 1970.
7. Stewartson, K. and Williams, P. G., "Self-Induced Separation", Proc. Royal Soc., Series A, Vol. 312, No. 1509, Sept. 1969.
8. Brown, S. N. and Stewartson, K., "Trailing-Edge Stall", J. Fluid Mech., Vol. 42, Part 3, 1970.
9. Messiter, A. F., Feo, A., and Melnik, R. E., "Shock Wave Strength for Separation of a Laminar Boundary Layer at Transonic Speeds", AIAA J., Vol. 9, No. 6, June 1971.
10. Brilliant, H. M. and Adamson, T. C., Jr., "Shock Wave-Boundary Layer Interactions in Laminar Transonic Flow", Paper No. 73-239, AIAA 11th Aerospace Sciences

Meeting, Washington, D. C., Jan. 1973.
11. Roshko, A. and Thomke, G. J., "Supersonic, Turbulent Boundary-Layer Interaction with a Compression Corner at Very High Reynolds Number", Douglas Paper 10163, McDonnell Douglas Astronautics Co., Western Div., May 1969.
12. Elfstrom, G. M., "Turbulent Hypersonic Flow at a Wedge-Compression Corner," J. Fluid Mech., Vol. 53, part 1, 1972.
13. Watson, E. C., Murphy, J. D. and Rose, W. C., "Investigation of Laminar and Turbulent Boundary Layers Interacting with Externally Generated Shock Waves," NASA TN D-5512, Nov. 1969.
14. Rose, W. C., "A Method for Analyzing the Interaction of an Oblique Shock Wave with a Boundary Layer", NASA TN D-6083, 1970.
15. Mellor, G. L., "The Large Reynolds Number, Asymptotic Theory of Turbulent Boundary Layers", Int. J. Eng. Sci., Vol. 10, 1972.
16. Yajnik, K., "Asymptotic Theory of Turbulent Shear Flows", J. Fluid Mech., Vol. 42, part 2, 1970.
17. Bush, W. B. and Fendell, F. E., "Asymptotic Analysis of Turbulent Channel and Boundary-Layer Flow", J. Fluid Mech., Vol. 56, part 4, 1972.
18. Bush, W. B. and Fendell, F. E., "Asymptotic Analysis of Turbulent Channel Flow for Mean Turbulent Energy Closures", Phys. Fluids, Vol. 16, No. 8, Aug. 1973.
19. Afzal, N., "A Higher-Order Theory for Compressible Turbulent Boundary Layers at Moderately Large Reynolds Number", J. Fluid Mech., Vol. 57, part 1, 1973.
20. Murman, E. M. and Cole, J. D., "Calculation of Plane Steady Transonic Flows", AIAA J., Vol. 9, Jan. 1971.
21. Adamson, T. C., Jr. and Feo, A., "Interaction Between a Shock Wave and a Turbulent Boundary Layer in Transonic Flow", to be published in SIAM J. Appl. Math.
22. Inger, G. R. and Mason, W. H., "Inviscid Small-Disturbance Theory for Nonuniform Transonic Flows", VPI-E-73-19, College of Engineering, Virginia Polytechnic Institute and State University, May 1973.
23. Coles, D. E. and Hirst, E. A. (ed.), Proceedings of the AFOSR-IFP Stamford Conference, Vol. 2, 1968.
24. Bradshaw, P. and Ferriss, D. H., "Calculation of Boundary-Layer Development Using the Turbulent Energy Equation: Compressible Flow on Adiabatic Walls", J. Fluid Mech., Vol. 46, part 1, 1971.
25. Kistler, A. L., "Fluctuation Measurements in a Supersonic Turbulent Boundary Layer", Phys. Fluids, Vol. 2, No. 3, 1959.
26. Bradshaw, P., "Anomalous Effects of Pressure Gradient on Supersonic Turbulent Boundary Layers", Imperial College of Science and Technology, I. C. Aero Rept. 72-21, Nov. 1972.
27. Bradshaw, P., "Effects of Streamline Curvature on Turbulent Flow", AGARD-AG-169, 1973.
28. Rotta, J. C., "Turbulent Boundary Layers with Heat Transfer in Compressible Flow", Agard Rept. 281, 1960.
29. Van Driest, E. R., "Turbulent Boundary Layer in Compressible Fluids", J. Aero Sci., Vol. 18, No. 3, March 1951.
30. Maise, G. and McDonald, H., "Mixing Length and Kinematic Eddy Viscosity in a Compressible Boundary Layer", AIAA J., Vol. 6, No. 1, Jan. 1968.
31. Alber, I. E. and Coats, D. E., "Analytical Investigations of Equilibrium and Nonequilibrium Compressible Turbulent Boundary Layers", AIAA J., Vol. 9, No. 5, May 1971.
32. Lagerstrom, P. A. and Casten, R. G., "Basic Concepts Underlying Singular Perturbation Techniques", SIAM Review, Vol. 14, No. 1, Jan. 1972.
33. Adams, M. C., "On Shock Waves in Inhomogeneous Flow", J. Aero. Sci., Vol. 10, No. 11, Nov. 1949.
34. Townsend, A. A., "The Behavior of a Turbulent Boundary Layer Near Separation", J. Fluid Mech., Vol. 12, 1962.
35. Seebass, R., Murman, E. M. and Krupp, J. A., "Finite Difference Calculation of the Behavior of a Discontinuous Signal Near a Caustic", Boeing Sci. Res. Lab. Doc. D1-82-1040, Jan. 1971.
36. Gadd, G. E., "Interactions Between Normal Shock Waves and Turbulent Boundary Layers", A.R.C. 22559, R & M 3262, 1962.
37. Vidal, R. J., Wittliff, C. E., Catlin, P. A. and Sheen, B. H., "Reynolds Number Effects on the Shock Wave-Turbulent Boundary Layer Interaction at Transonic Speeds", Paper No. 73-661, AIAA 6th Fluid and Plasma Dyn Conf., Palm Springs, California, July 1973.
38. Seddon, J., "The Flow Produced by Interaction of A Turbulent Boundary Layer with a Normal Shock Wave of Strength Sufficient to Cause Separation", R.A.E. Tech. Memo Aero 667 (A.R.C. 22637, R & M 3502), 1960.

Appendix A. Matching of the Non-interacting Velocity Profiles

In this appendix, we consider the Maise-McDonald[30] profile given by eqs. (3.1) through (3.5) as an exact solution, and show that the usual limit-function expansions do not overlap. Expanding (3.1) and (3.4) in powers of ϵ with y fixed, we obtain

$$u_{outer} = 1 + \epsilon u_1 - \epsilon^2 \tfrac{1}{2} m_e u_1^2 + \cdots \qquad (A.1)$$

where

$$u_1 = \frac{1}{\kappa} \log y - \frac{\bar{\pi}}{\kappa} (1 + \cos \pi y) \qquad (A.2)$$

The inner (limit-function) expansion is obtained by expanding (3.1) and (3.5) for small ϵ holding y^* fixed, whereby

$$u_{inner} = \epsilon u_1^* - \tfrac{1}{6} \epsilon^3 \left(\frac{m_e}{1 + m_e} \right) u_1^{*3} + \cdots \qquad (A.3)$$

with

$$u_1^* = \frac{1}{\kappa} \log y^* + B_0 \qquad (A.4)$$

In order to demonstrate matching, we must compare the inner expansion of the outer solution with the outer expansion of the inner solution. Carrying out these constructs and expressing both expansions in the outer variable y, we obtain

$$\text{Inner}[u_{outer}] = 1 + g_1 + 0(\epsilon^2) \qquad (A.5)$$

$$\text{Outer}[u_{inner}] = (\tilde{u}_e - \tfrac{1}{6} a \tilde{u}_e^3 + \cdots) + \epsilon (1 - \tfrac{1}{2} a \tilde{u}_e^2 + \cdots) g_1 + 0(\epsilon^2) \qquad (A.6)$$

where

$$g_1 = \frac{1}{\kappa} \log y - \frac{2\bar{\pi}}{\kappa} \qquad (A.7)$$

The coefficients of eq. (A.6) can be shown to be an infinite series in powers of $(a\tilde{u}_e)$ arising from contributions of higher order terms in the inner solution. Comparison of eqs. (A.5) and (A.6) shows that the inner and outer limit function expansions do not match for non-zero M_e. Analysis using the more general notation of intermediate variables, (e.g. see Ref. 32) indicates that this difficulty cannot be rectified since the domain of validity of the two expansions does not overlap.

The matching problem can be viewed as being caused by the simple expansion of the trigonometric terms in the inner solution. Such an expansion implies that the density is a constant, equal to the wall value, in the lowest-order solution. The problem is resolved by assuming that the solution in the wall layer is given by the full expressions in eqs. (3.1) and (3.5). We now show that the generalized inner expansion matches the outer limit-function expansion given by eq. (A.1).

To demonstrate matching, we write the full wall layer solution in outer variables

$$u_{inner} = \frac{1}{a} \sin a \left\{ \tilde{u}_e + \frac{\epsilon}{\sqrt{\rho_w}} \left[\frac{1}{\kappa} \log y - \frac{2\bar{\pi}}{\kappa} (1 - \cos \pi y) \right] \right\} \qquad (A.8)$$

We assume this solution is valid in a domain $y^* \to \infty$ such that

$$0(\epsilon \log y) < 0(1)$$

This allows us to expand Eq. (A.8) for small $\epsilon \log y$ which results in the following large y^* solution:

$$\text{Outer}[u_{inner}] = 1 + \epsilon u_1 - \epsilon^2 \frac{m_e}{2} u_1^2 \qquad (A.9)$$

Comparison of this last result with eq. (A.1) demonstrates that the generalized inner solution matches the outer (limit-function) expansion.

This demonstrates that the Maise-McDonald correlation does provide an initial profile that is consistent with the asymptotic formulation of compressible turbulent boundary layers. In this analysis, we assume the initial profile to be given by eqs. (3.1) through (3.5). This will allow a rational two parameter fit of specified experimental profiles. We also note that the profiles can be represented by asymptotic expansions given by Eq. (A.1) in the outer region and by eq. (3.5) with the $\bar{\pi}$ terms neglected in the fully turbulent part of the inner region.

Appendix B. Solution of the Outer Layer for $\chi_t \to 0$

The outer-layer equations given by eq. (4.14) should reduce to Adamson and Feo's[21] weak shock theory in the limit $\chi_t \to 0$. The approach to this limit is somewhat complicated and involves the splitting of the outer inviscid region into two inviscid layers. One layer consists of the main part of the defect region and is scaled by the boundary-layer thickness. The streamwise scale must be stretched by χ_t as follows

$$x = \hat{x} / \sqrt{\chi_t} \qquad (B.1)$$

The y coordinate remains unchanged. Thus, inner variables are given by $\hat{x}$, and y. Eq. (B.1) indicates that the streamwise length scale increases as χ_t gets small and this implies that normal pressure gradients in the defect layer will vanish to lowest order as $\chi_t \to 0$. In this inner region, ϕ should be expanded in the form

$$\phi = \sqrt{\chi_t}\,[\phi_0(\hat{x}) + \chi_t \phi_1(\hat{x}, y) + \cdots] \qquad (B.2)$$

Substituting eqs. (B.1) and (B.2) into eq. (4.14) and imposing the boundary condition

$$\phi_{1_y}(\hat{x}, 0) = 0$$

leads to the following solution ϕ_{1_y}:

$$\phi_{1_y} = \phi_{0\hat{x}\hat{x}} \int_0^y \lambda(y)dy \qquad (B.3)$$

where at this stage of the solution $\phi_{0\hat{x}\hat{x}}$ is an arbitrary function and λ is defined in eq. (4.15). The above solution implies that the pressure is constant in the defect layer and is given by

$$\hat{p}_0 = \hat{p}_{0_\infty}(\hat{x}) = -\phi_{0\hat{x}} \qquad (B.4)$$

Thus, eq. (B.3) provides a relationship between the normal component of velocity and the pressure gradient

$$\hat{V}_1 = \phi_{1_y} = -\frac{d\hat{p}_{1_\infty}}{d\hat{x}} \int_0^y \lambda(y)dy \qquad (B.5)$$

eq. (B.5) is the defect layer solution derived in Ref. 21. Notice that $\hat{V}_1$ approaches a non-zero limit as y approaches infinity,

$$\hat{V}_1(x, \infty) = \hat{V}_{1_\infty} = -\frac{d\hat{p}_{1_\infty}}{d\hat{x}} \int_0^\infty \lambda(y)dy \qquad (B.6)$$

Thus the inner solution cannot satisfy the outer boundary conditions and an outer solution is required for large y. Analysis indicated that the appropriate outer variable is

$$y = \hat{y}/\chi_t \qquad (B.7)$$

In order to match the defect solution in eq. (B.6), we must stretch the potential

$$\phi = \sqrt{\chi_t}\,\hat{\phi} \qquad (B.8)$$

Substitution of outer variable $\hat{x}$, $\hat{y}$, $\hat{\phi}$ into eqs. (4.14) and setting χ_t to zero results in the following equation:

$$[1 + (\gamma+1)\hat{\phi}_{\hat{x}}]\hat{\phi}_{\hat{x}\hat{x}} - \hat{\phi}_{\hat{y}\hat{y}} = 0 \qquad (B.9)$$

This is the transonic small disturbance equation which Adamson and Feo showed to govern their outer solution. Equation (B.9) must be solved subject to the boundary conditions

$$\hat{\phi}_{\hat{y}} - \hat{\phi}_{\hat{x}\hat{x}} \int_0^\infty \lambda(y)dy = 0 \text{ for } \hat{y} \to 0$$
$$\hat{\phi}_{\hat{x}} \to 0 \text{ for } \hat{x} \to -\infty \qquad (B.10)$$

which is derived by matching the inner and outer solutions. The problem formulation is completed by specifying boundary conditions for large y. The boundary value problem consisting of eqs. (B.9) and (B.10) and the outer boundary conditions determined by the incoming wave, is precisely the problem arrived at in Ref. 21. They showed a turbulent free interaction solution can be derived by using a simple wave solution of eq. (B.9).

In the notation of the present paper, their free interaction solution can be written in the form

$$p_{1_w} = -\frac{\chi_t}{\gamma+1}[Z - 1]$$
$$x = \text{Constant} + A\sqrt{\frac{\gamma+1}{\chi_t}}\left\{\tfrac{1}{3}\log\frac{(1 - Z^{1/2})^2}{1 + Z + Z^{1/2}} + \frac{2}{\sqrt{3}}\tan^{-1}\left(\frac{2Z^{1/2}+1}{\sqrt{3}}\right)\right\} \qquad (B.11)$$

where A is the constant appearing in Ref. 21 and is given by

$$A = -\tfrac{1}{2}\sqrt{\gamma+1}\int_0^\infty \lambda(y)dy \qquad (B.12)$$

or using eqs. (3.13) and (4.15)

$$A = \frac{3}{2\kappa}\sqrt{\gamma+1}(\bar{\imath}+1) \qquad (B.13)$$

The free interaction solutions given in eq. (B.11) form a one-parameter family of solutions corresponding to an arbitrary shift of the origin.

The solution given by eq. (B.11) leads to a surface pressure distribution that rises smoothly from free stream pressure at negative infinity to sonic pressure at the downstream terminus of the solution. The pressure gradient rises monotonically from zero at negative infinity to a finite value at the sonic point. The second derivative is positive over the entire interval of definition of the solution. From this last property, it can be shown that the simple wave pattern does not involve a focusing of characteristics nor a formation of an imbedded shock wave. It also follows that the wave pattern is terminated downstream by

an envelope (or caustic) of the straight-line characteristics. The envelope, which is convex to the supersonic region, starts off normal to the x-axis at the sonic point and is asymptotic to a straight line inclined at the free-stream characteristic direction at positive infinity. The implications of these properties of the free-interaction solution on the wave pattern in shock wave-boundary layer interactions are discussed in section IX of this paper.

Appendix C. Matching of the Blending and Wall-Layer Solutions

The wall-layer solution using Van Driest's generalized velocities will be shown to match the solution in the blending layer. The requirement that the two expansions match, leads to a corresponding solution for the skin friction, which will be derived in this appendix. Since the wall-layer solution is not in the form of a limit-function expansion, matching of the two expansions requires some special steps. First, we write the generalized wall-layer solution given by eq. (6.27) in terms of the blending-layer variable y. The definition of the stretched variables y and y^* and the skin-friction law for the non-interacting flow can be used to establish the following relationship between y and y^*:

$$\frac{1}{\kappa}\log y^* + B_0 = \frac{\sqrt{\rho_{w0}}}{\epsilon}\tilde{u}_e + \frac{3}{2\kappa}\log\epsilon + H(Y) \quad (C.1)$$

where H(Y) is the function defined in eq. (5.14). Equation C.1 is used to express all y^* terms appearing in the wall-layer solution for u, eq. (6.21) in terms of the blending-layer variable Y. The result can be written in the form

$$u = \frac{1}{a}\sin\left[a\tilde{u}_e + \frac{a}{\sqrt{\rho_{w0}}}G(Y;\epsilon)\right] \quad (C.2)$$

or, expanding the trigonometric terms and using the definition of $\tilde{u}_e$

$$u = \cos\left[\frac{a}{\sqrt{\rho_{w0}}}G(Y;\epsilon)\right] + \frac{\sqrt{\rho_{w0}}}{a}\sin\left[\frac{a}{\sqrt{\rho_{w0}}}G(Y;\epsilon)\right] \quad (C.3)$$

The function G is given by

$$\begin{aligned} G = {} & \frac{3}{2\kappa}\epsilon\log\epsilon + \epsilon\left\{H(Y) + \tfrac{1}{2}(\tau_{w1} - \rho_{w1})q\right\} \\ & + \epsilon^2\log\epsilon\left\{\tfrac{1}{2}q\tau_{w21} + \frac{3}{4\kappa}(\tau_{w1} - \rho_{w1})\right\} \\ & + \epsilon^2\left\{\tfrac{1}{2}(\tau_{w1} - \rho_{w1})(H - B_0) + \frac{q}{2}\left[\tau_{w22} - \rho_{w2}\right.\right. \\ & \left.\left. + \rho_{w1}^2 - \tfrac{1}{4}(\tau_{w1} - \rho_{w1})^2\right]\right\} \end{aligned} \quad (C.4)$$

One of the principal consequences of the large Reynolds number limit is the fact that the total shear stress, laminar plus turbulent, is constant to all orders in ϵ across the wall layer. Analysis of the error terms in the wall-layer equations indicate that the main error terms for large y^* arise from variations of total stress. It follows from consideration of these terms that the generalized wall-layer solution is valid in a region defined by

$$\left.\begin{array}{l}\epsilon \to 0 \\ y^* \to \infty\end{array}\right\} \text{ such that } 0[\epsilon H(Y)] < 0(1) \quad (C.5)$$

It follows from this result that the function G defined in eq. (C.4) vanishes for $\epsilon \to 0$ in this region. Hence, an outer expansion of the inner solution, valid in the region defined by eq. (C.5), can be obtained by expanding eq. (C.3) for small G. This yields, to terms of second order

$$\begin{aligned} \text{Outer (Blending-Layer) } [u_{\text{inner}}] = {} & 1 + \frac{3}{2\kappa}\epsilon\log\epsilon \\ & + \epsilon\left[H(Y) + \frac{q}{2}(\tau_{w1} - \rho_{w1})\right] - \epsilon^2\log^2\epsilon\left[\frac{m_e}{2}\left(\frac{3}{2\kappa}\right)^2\right] \\ & + \epsilon^2\log\epsilon\left\{\frac{q}{2}\tau_{w21} + \frac{3}{4\kappa}(\tau_{w1} - \rho_{w1})\right. \\ & \left. - \frac{3m_e}{2\kappa}\left[H(Y) + \frac{q}{2}(\tau_{w1} - \rho_{w1})\right]\right\} - \epsilon^2\left\{\frac{m_e}{2}H^2(Y)\right. \\ & + \tfrac{1}{2}(m_e q - 1)(\tau_{w1} - \rho_{w1})H(Y) + \frac{q}{8}(1 + m_e q) \\ & \times (\tau_{w1} - \rho_{w1})^2 + \tfrac{1}{2}B_0(\tau_{w1} - \rho_{w1}) \\ & \left. - \frac{q}{2}(\tau_{w2} - \rho_{w2} + \rho_{w1}^2)\right\} \end{aligned} \quad (C.6)$$

The previous result is to be compared with the inner expansion of the blending-layer solution. This is obtained by substituting eq. (5.28) into eq. (5.7) which yields:

$$\begin{aligned} \text{Inner } [u_{\text{blending layer}}] = {} & 1 + \frac{3}{2\kappa}\epsilon\log\epsilon \\ & + [H(Y) - P_1] - \epsilon^2\log^2\epsilon\frac{m_e}{2}\left(\frac{3}{2\kappa}\right)^2 \\ & + \epsilon^2\log\epsilon\left[(1 + 2m_e)\left(\frac{3}{2\kappa}\right)P_1 - \frac{3m_e}{2\kappa}H(Y)\right] \\ & - \epsilon^2\left[\frac{m_e}{2}H^2(Y) - \tfrac{1}{2}(\tau_{w1} - M_e^2 P_1)H(Y) + P_2 - C_2\right] \end{aligned} \quad (C.7)$$

Analysis of error terms indicate that this expansion is valid in the domain defined by

$$\left.\begin{matrix}\epsilon \to 0 \\ Y \to 0\end{matrix}\right\} \text{ such that } 0(\epsilon \log Y) < 0(1) \qquad \text{(C. 8)}$$

This can be shown to overlap with the region of validity of the wall layer defined by eq. (C. 5). Thus, eqs. (C. 6) and (C. 7) can be matched term by term and the introduction of intermediate variables[32] is not required for this problem. Taking note that the pressures match, the requirement that eq. (C. 6) and (C. 7) match yields the following expressions for the first three terms of the skin friction solution:

$$\tau_{w1} = \left(\gamma M_\infty^2 - \frac{2}{q}\right) p_{w1}$$

$$\tau_{w21} = \frac{3}{\kappa q^2}\left[1 + (1 + m_\infty)q\right] p_{w1}$$

$$\tau_{w22} = \frac{2C_2}{q} + \left(\gamma M_\infty^2 - \frac{2}{q}\right) p_{w2} + \left(\frac{1 + m_\infty q}{q^2} - \gamma^2 M_\infty^4\right) p_{w1}^2 - \frac{2B_0}{q^2} p_{w1} \qquad \text{(C. 9)}$$

Substitution of these results in eq. (6. 22) leads to the skin-friction solution given in eq. (6. 28).

We note that the expansion for the skin friction, eq. (6. 28), contains a sequence of terms that proceed in powers of the function $(\epsilon \gamma M_\infty^2 p_{w1})$. Because of these terms, the formal expansion for the skin friction approaches its large Reynolds number limit very slowly, and is useful only for very small free stream Mach numbers (e. g. $M_\infty < 0.5$). These terms arise from the expansion in powers of ϵ of the wall density written as a function of the surface pressure. Thus, they arise only in compressible flows with pressure gradients. The utility of the formal solution for the skin friction can be improved by a Euler summation of these terms. The rearranged solution can then be written in the form

$$\frac{c_f}{c_{f_0}} = \left[2 - \frac{\rho_{w(0)}}{\rho_{w(\epsilon,\epsilon)}}\right] - \epsilon \frac{2}{q} p_{w1} + 3\epsilon^2 \log\epsilon \left[\frac{1 + (1 + m_\infty)q}{q^2 \kappa}\right] p_{w1} - \epsilon^2 \left[\frac{2}{q} p_{w2} - \frac{(1 + m_\infty q)}{q^2} p_{w1}^2 + \frac{2B_0}{q^2} p_{w1} - \frac{2C_2}{q}\right] \qquad \text{(C. 10)}$$

where

$$\frac{\rho_{w(0)}}{\rho_{w(\epsilon,\epsilon)}} = \left\{1 + \epsilon \gamma M_\infty^2 \left[p_{w1} + \epsilon p_{w2} + \cdots\right]\right\}^{-1} \qquad \text{(C. 11)}$$

In the above rearranged series, the wall density terms are effectively summed to all orders in ϵ. Notice that contributions from the wall density, in the second term of the above solution, now vary between one for $M_\infty = 0$ and zero for $M_\infty \to \infty$. Previously, these terms became unbounded as the Mach number approached infinity.

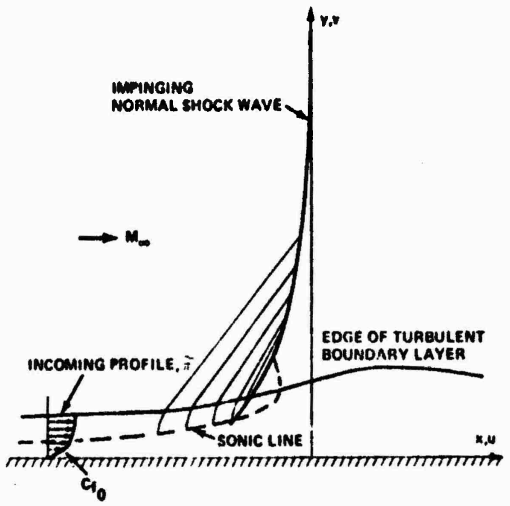

FIG. 1 SCHEMATIC OF SHOCK WAVE – TURBULENT BOUNDARY LAYER INTERACTION

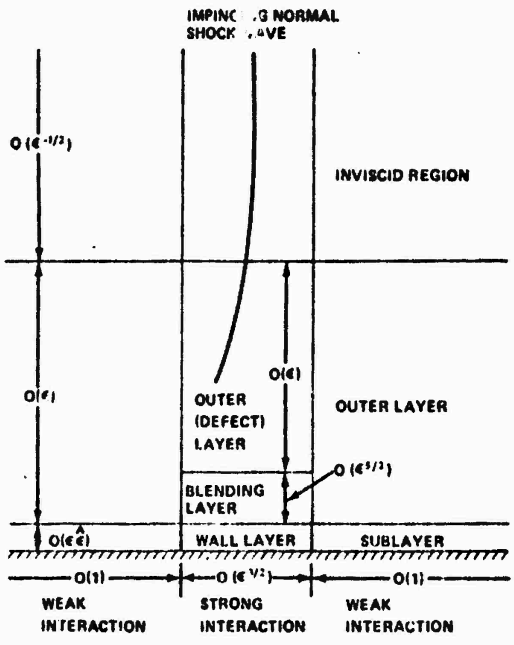

FIG. 2 ASYMPTOTIC FLOW – FIELD STRUCTURE

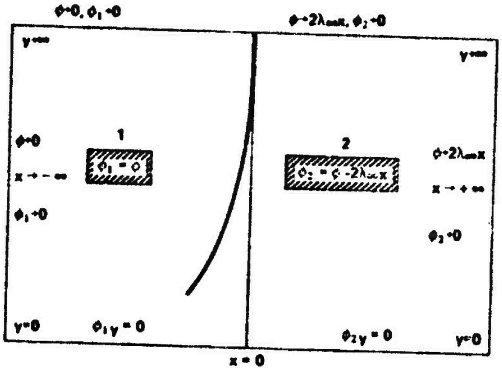

FIG. 3 BOUNDARY-VALUE FORMULATION OF INTERACTING OUTER-LAYER EQUATIONS

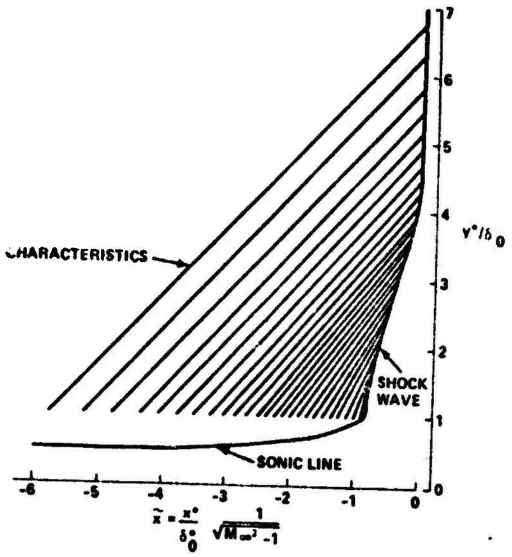

FIG. 5 COMPUTED SHOCK SHAPE, SONIC LINE AND CHARACTERISTICS, $x_t = 7.5$, $\bar{\tau} = 0.5$

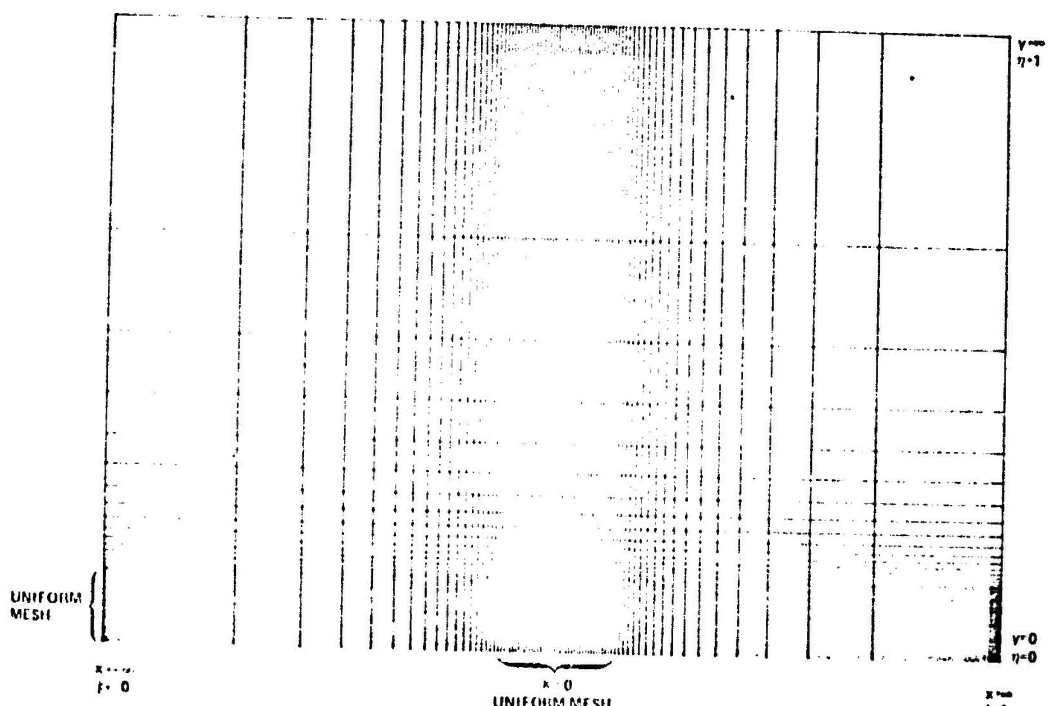

FIG. 4 COMPUTATIONAL MESH POINT DISTRIBUTION, INTERACTING OUTER LAYER EQUATIONS

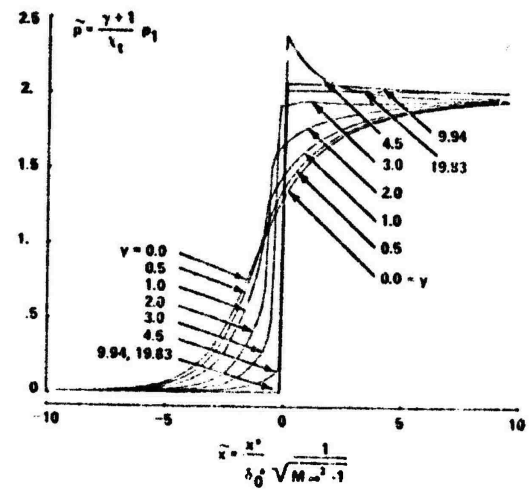

FIG. 6 DEFECT PRESSURE DISTRIBUTIONS, $\chi_t = 7.5$, $\tilde{x} = 0.5$

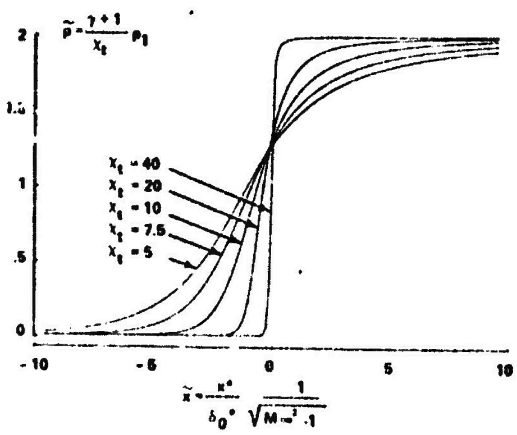

FIG. 8 SURFACE DEFECT PRESSURE DISTRIBUTION vs χ_t, $\tilde{x} = 0.5$

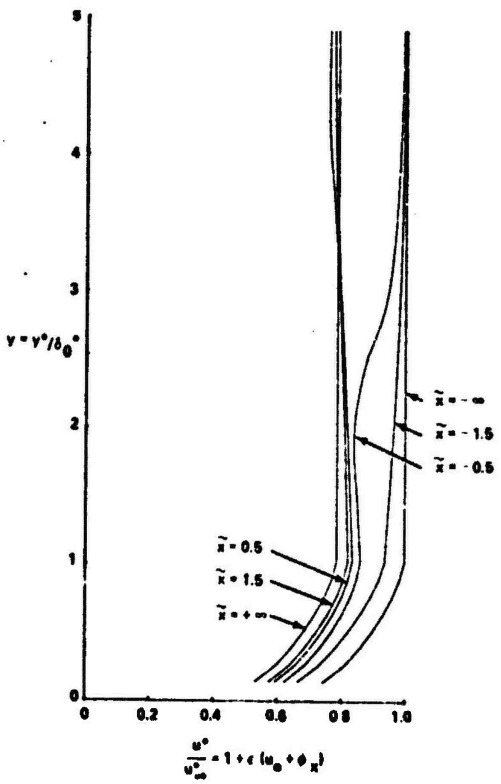

FIG. 7 VELOCITY PROFILES, $\chi_t = 7.5$, $\tilde{x} = 0.5$

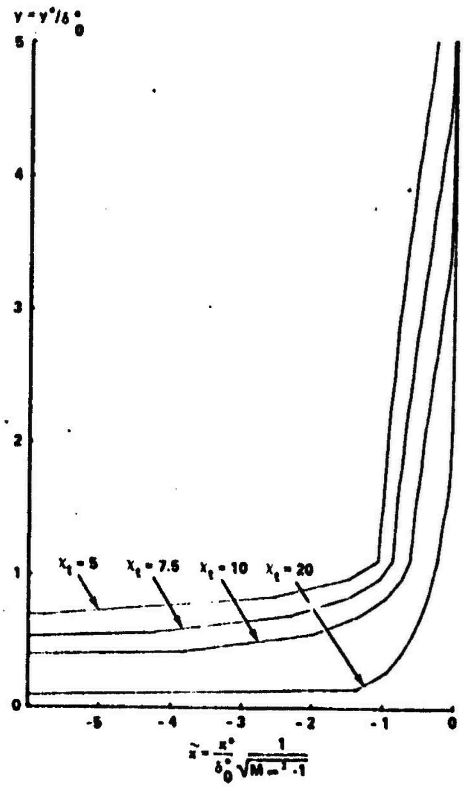

FIG. 9 SHOCK SHAPE AND SONIC LINE vs χ_t, $\tilde{x} = 0.5$

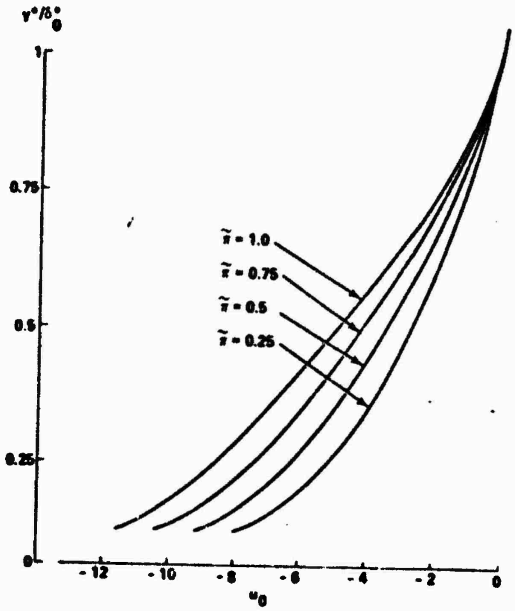

FIG. 10 NON-INTERACTING DEFECT VELOCITY PROFILES vs $\tilde{\pi}$

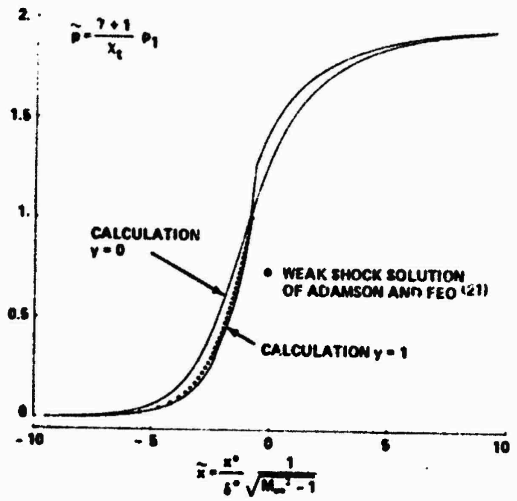

FIG 12 DEFECT PRESSURE COMPARED TO WEAK SHOCK ANALYSIS, χ_t = 7.5

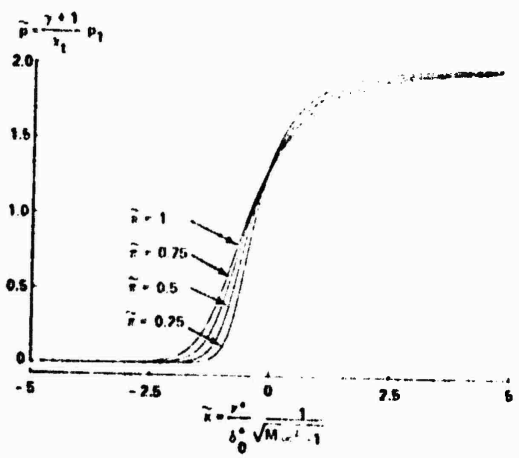

FIG. 11 SURFACE DEFECT PRESSURE DISTRIBUTIONS vs $\tilde{\pi}$, χ_t = 20

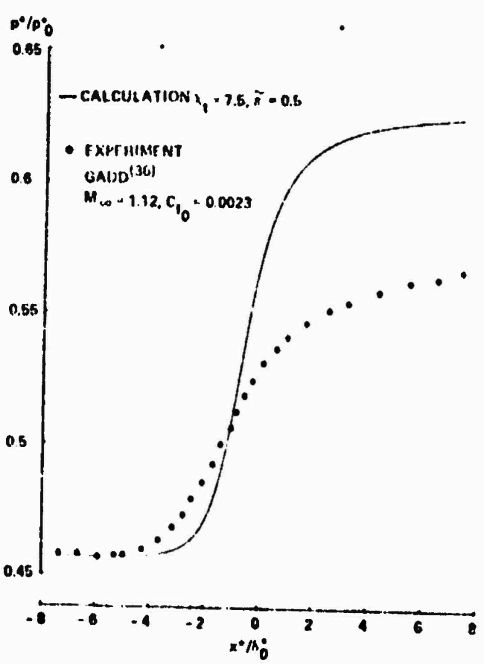

FIG 13 DEFECT PRESSURE COMPARED TO EXPERIMENT, χ_t = 7.5

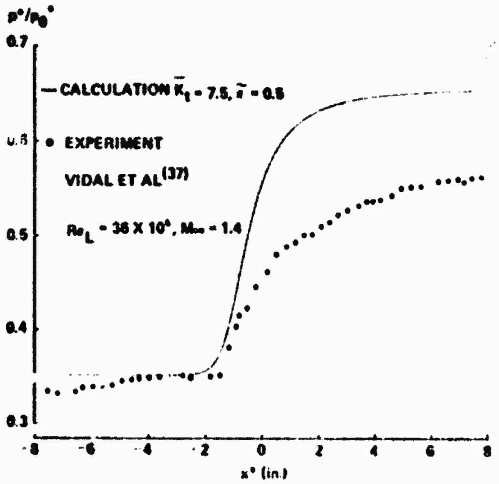

FIG. 14 SURFACE PRESSURE COMPARED TO EXPERIMENT, $\bar{K}_1 = 7.5$

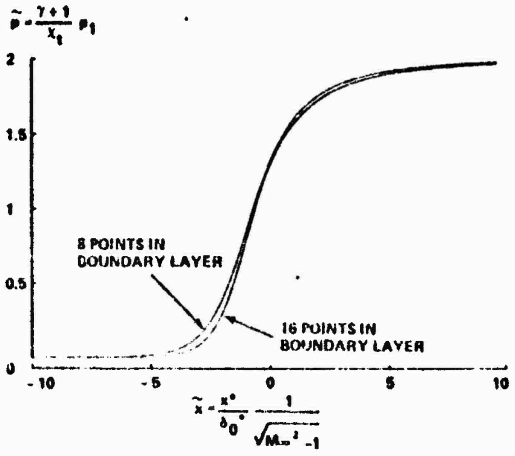

FIG. 15 EFFECT OF MESH DISTRIBTUION ON SURFACE DEFECT PRESSURES AT $\bar{x}_1 = 10, \tilde{x} = 0.5$